AD-A188 720 ON THE THEORY OF ELECTROMAGNETIC SCATTERING FROM A RAINDROP SPLASH(U) NAVAL RESEARCH LAB WASHINGTON DC L B WETZEL 31 DEC 87 1/1

UNCLASSIFIED F/G 20/3 NL

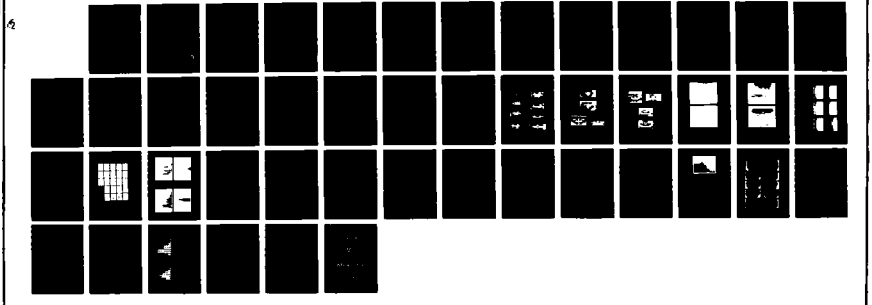

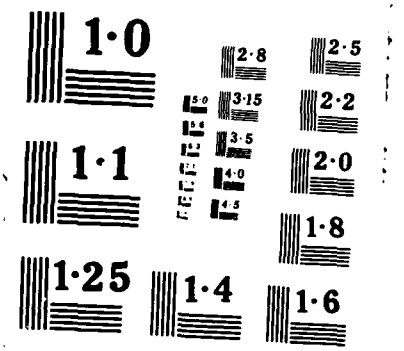
1·0
1·1
1·25
1·4
1·6
1·8
2·0
2·2
2·5
2·8
3·15
3·5
4·0
4·5

Naval Research Laboratory
Washington, DC 20375-5000

NRL Memorandum Report 6103

On the Theory of Electromagnetic Scattering from a Raindrop Splash

L. B. WETZEL

Senior Scientist and Propagation Staff
Radar Division

December 31, 1987

SECURITY CLASSIFICATION OF THIS PAGE

REPORT DOCUMENTATION PAGE

Form Approved
OMB No. 0704-0188

1a REPORT SECURITY CLASSIFICATION UNCLASSIFIED	1b RESTRICTIVE MARKINGS A188 720
2a SECURITY CLASSIFICATION AUTHORITY	3 DISTRIBUTION / AVAILABILITY OF REPORT Approved for public release; distribution unlimited.
2b DECLASSIFICATION / DOWNGRADING SCHEDULE	
4 PERFORMING ORGANIZATION REPORT NUMBER(S) NRL Memorandum Report 6103	5 MONITORING ORGANIZATION REPORT NUMBER(S)
6a NAME OF PERFORMING ORGANIZATION Naval Research Laboratory 6b OFFICE SYMBOL (If applicable) Code 5303	7a NAME OF MONITORING ORGANIZATION Office of Naval Research
6c ADDRESS (City, State, and ZIP Code) Washington D.C. 20375-5000	7b ADDRESS (City, State, and ZIP Code) Arlington, VA 22217
8a NAME OF FUNDING / SPONSORING ORGANIZATION Office of Naval Research 8b OFFICE SYMBOL (If applicable)	9 PROCUREMENT INSTRUMENT IDENTIFICATION NUMBER
8c ADDRESS (City, State, and ZIP Code) Arlington, VA 22217	10 SOURCE OF FUNDING NUMBERS PROGRAM ELEMENT NO: 61153N PROJECT NO: RR021-05-43 TASK NO: WORK UNIT ACCESSION NO: DN 280-045

11 TITLE (Include Security Classification)
On the Theory of Electromagnetic Scattering from a Raindrop Splash

12 PERSONAL AUTHOR(S)
Wetzel, Lewis B.

13a TYPE OF REPORT	13b TIME COVERED FROM ____ TO ____	14 DATE OF REPORT (Year, Month, Day)	15 PAGE COUNT
		1987 December 31	46

16 SUPPLEMENTARY NOTATION

17 COSATI CODES			18 SUBJECT TERMS (Continue on reverse if necessary and identify by block number)
FIELD	GROUP	SUB GROUP	Rain Splash Scatter, Sea Clutter, Radar Clutter, Sea Scatter, Rain Scatter

19 ABSTRACT (Continue on reverse if necessary and identify by block number)

Electromagnetic scattering from a raindrop splash on a water surface is examined in terms of the splash structures that have been disclosed by high-speed photography. Of the three basic scattering features, the "crown," the "stalk," and the "ring wave," the first two are modeled as dielectric cylinders, while the third is treated by a perturbation approximation. Cross section predictions based on these models are found to be in good agreement with Hansen's laboratory measurements of splash scattering. Procedures are given for extending these models to natural rain falling on "calm" water surfaces, although the present lack of sufficiently complete experimental data prevents direct verification of the theory. Nevertheless, a few qualitative conclusions can be drawn from the formalism: the major scattering feature is the stalk, and while the vertically polarized returns will have only a weak dependence on rain rate, the horizontally polarized returns will depend strongly on both the rain rate and the shape of the stalk (or drop) size distribution curves. Recognizing that comprehensive field measurements of splash scattering on calm water would be difficult to accumulate, several additional laboratory experiments are suggested.

20 DISTRIBUTION / AVAILABILITY OF ABSTRACT	21 ABSTRACT SECURITY CLASSIFICATION
☒ UNCLASSIFIED/UNLIMITED ☐ SAME AS RPT ☐ DTIC USERS	UNCLASSIFIED
22a NAME OF RESPONSIBLE INDIVIDUAL Lewis B. Wetzel	22b TELEPHONE (Include Area Code) (202) 767-3417
	22c OFFICE SYMBOL Code 5303

DD Form 1473, JUN 86 Previous editions are obsolete SECURITY CLASSIFICATION OF THIS PAGE

S/N 0102-LF-014-6603

CONTENTS

I. INTRODUCTION 1

II. THE SPLASH PROCESS 1

III. SPLASH SCATTERING EXPERIMENTS 2

IV. MODELING CROWN AND STALK SCATTER 3

A. Application of the Metallic Cylinder Model 4
B. A Dielectric Waveguide Model of the Stalk 5

V. SCATTERING BY THE RING WAVE 6

A. Characteristics of the Ring Wave 7
B. A Perturbation Theory of Ring Wave Scattering 7

VI. PREDICTION OF THE RAIN-RATE DEPENDENCE OF SPLASH SCATTER 8

A. The Stalk-Height Distribution 8
B. The Effects of Surface Slopes 9
C. Calculating the Average Cross Section 9

VII. SUMMARY AND CONCLUSIONS 11

REFERENCES 13

APPENDIX 15

ON THE THEORY OF ELECTROMAGNETIC SCATTERING FROM A RAINDROP SPLASH

I. INTRODUCTION

Interest in electromagnetic scattering by splashes derives primarily from interest in the effect of rain on radar sea backscatter. Radar operators will tell you that rain tends to suppress sea backscatter, and the observations of operators should always be taken seriously. Yet there has been little in the way of reliable, quantitative experimental information about the interaction between rain and rain-driven sea backscatter, and no real theory whatsoever. Laboratory measurements by Moore, et al, [1979] with artificial "rain" suggested that for light "winds" the backscatter level increased with rain rate, while for heavy winds rain made little difference. In measurements in natural rain over the Chesapeake Bay, Hansen [1984] found that even a light rain (2 mm/hr) changes the spectral character of sea backscatter at moderate wind speeds (6 m/sec) by introducing a significant high frequency component. He also found some evidence in support of the radar operators at low grazing angles with horizontal polarization, which is the most common operating regime for Navy radars. Since these two studies constitute the total published effort on this problem, an understanding of the complex phenomenology of rain/sea-scatter interactions will have to be approached essentially from scratch.

This paper takes a first step by developing a model for scattering from an isolated splash and applying this model to a statistical description of the radar cross section of natural rain splashes on a "calm" water surface.

II. THE SPLASH PROCESS

Not everyone likes the rain, but there are few who have not wondered at the unexpected display of a raindrop falling on a water surface — the explosive jet rising from the center, the fleeting silver ring that vanishes almost before you realize what it is. Over 100 years ago, his fascination with this event led Worthington [1882, 1962] to develop a remarkable photographic system for recording the process with millisecond precision, using "state-of-the-art" equipment of his day. His raindrop was a ball of water rolled off a smoked watchglass, activated by a magnetic latch which also opened the shutter of a wet-plate camera whose emulsion he had freshly mixed. After a suitable delay, a bank of Leyden Jars was discharged into an arc to illuminate the scene with a flash of millisecond duration. Some examples of his wizardry are seen in Fig.1, where we see the three basic structures associated with a splash: the "crown," the "stalk" (or "plume" or "jet"), and the "ring wave." Since then, of course, the beauty and novelty of the event, captured easily by modern high-speed flash photography, have made stop-action and slow—motion photos of splashes familiar to almost everyone. A gallery of photos taken recently by Cavaleri [1985] is shown in Figs. 2 and 3.

It is clear from the photographic evidence that the splash process produces three well-defined structures whose dimensions seem to be related to the drop diameter D. They occur in time sequence, with the entire process proceding as follows: First a "crown" with an irregular upper boundary grows from the initial impact to a height of about 1 D and diameter of 3-4 D. The growth and decay of the "crown" lasts about 50 milliseconds, leaving an elevated ring of water moving out

Manuscript approved August 27, 1987

from the site with a central depression at its center. The floor of this central depression rises into a kind of cone, from which grows a "stalk" carrying a ball of liquid at its top. The stalk diameter seems to be about 3/4 D and reaches a maximum height of 4-6 D. Its growth and decay lasts 100-200 msec, and as it reaches its peak and starts to decay, the ball may be squeezed off, with the column separating into several droplets (Fig. 3) — or it may not (Fig. 2). The collapsing stalk produces a second annular wave that propagates outward in pursuit of the original "crown" wave, the whole thing preceded by what appears to be a set of waves of very small wavelength (parasitic capillaries?) If secondary droplets have been squeezed off in the stalk, they fall back to form much weaker systems of secondary "ring waves." Variations in the details of the splash process are probably due to variations in such parameters as surface and drop temperatures, surface cleanliness, drop size and velocity. For large, high-speed drops, for example, the walls of the "crown" are seen to meet over the top of the initial crater to form a "bubble."

The detailed hydrodynamics of the splash process is not well understood. In fact, the major reference for rain-like splashes remains the mostly descriptive work by Worthington cited above. The more recent work on splashes is directed toward special cases — e.g., high-velocity impacts [Engel, 1966], and low-angle sprays in which drops bounce off the surface like skipping stones [Jayaratne and Mason, 1964]. However, some insights into general splash dynamics may be found in these references. For example, in Engel's experiments the falling drop was dyed red, and white particles were suspended in the target water to help visualize the resulting internal flow patterns. It was found that the ball atop the "stalk" contained the red dye of the original falling drop, and that the growth and decay of the crown and the emergence of the stalk were associated with an oscillating toroidal vorticity. But knowledge of the physics of splashes is really not necessary for the development of scattering models. It is sufficient to to know the structural forms of the various parts of the splash, and photographic evidence of the type seen in the Figures above can provide this information.

III. SPLASH SCATTERING EXPERIMENTS

In the first recorded measurement of its kind, Hansen [1984] measured radar backscatter versus rain rate from a "calm" natural water surface. This was done over the Chesapeake Bay using an X-band radar with both horizontal and vertical polarizations. A patch of calm water surface was under illumination just as it started to rain, and as the rain intensity steadily increased, the record shown in Fig. 4 was obtained. While it is dangerous to generalize from a single measurement, it is clear that for this rain sample, at least, there was a strong polarization dependence at low rain rates, while at the higher rain rates, both polarizations reached backscatter levels equal to those for a moderate wind-driven sea at the same grazing angle (about -40 dBm^2/m^2 at 2° grazing.)

In order to determine the scattering cross sections of individual splashes, Hansen set up a laboratory experiment in which scattering from splashes produced in a laboratory tank by drops of known size was measured using a high-resolution time — domain reflectometer [1985, 1986]. This instrument recorded the time history of scattering from the entire splash process on a split-screen display, which showed this history updated at 17 msec intervals along with a snapshot of the instantaneous state of the developing splash. An example of such a sequence is given in Fig. 5 for vertically polarized backscatter. Figure 6 shows two pairs of records of the complete scattering process, with V-Pol on the top and H-Pol below, the first for a drop of 4mm diameter and the second for a 3mm drop. Drops of the same size tended to give similar results (observe the close similarity between the scattering profiles in Figs. 5 and 6a for the same size drop), so the differences between the 4mm and 3mm returns indicate the nature of drop-size sensitivities in the scattering process. It should be noted that the two polarizations could not be recorded simultaneously for the same drop, so the upper and lower records in Fig. 6 belong to two different drops of the same size. We will be discussing these records in greater detail in the next section.

This meager body of scattering data is about all there is at the present time, and the laboratory data cannot really be considered representative of natural rain, since the drops fell through distances short of those required to reach terminal velocity in the open air. Nevertheless, the splashes produced in the laboratory and in nature look very similar, and it is the look, rather than the detailed physics, of the splash process that we will use to guide our modeling efforts.

IV. MODELING CROWN AND STALK SCATTER

Both crown and stalk have cylindrical symmetry, so it is tempting to model them as finite water cylinders standing out of an infinite water surface. A full-scale boundary value problem even for this simple geometry would be quite difficult to solve, so we revert to an even simpler *ad hoc* model in which the cylinders are quasi-metallic (impenetrable) and the water surface enters simply as a reflecting plane with a prescribed relection coefficient.

The basic scattering geometry is shown in Fig. 7, where the scattering cylinder is represented by a stack of discs, each being a slice of an infinite cylinder illuminated from, and scattering into, the pair of possible paths created by the presence of the surface. The scattered field for each disc is written in terms of radial eigenfunction expansions appropriate to illumination of an infinite cylinder by plane waves arriving along the direct and surface-reflected paths and returning to the source along these same paths. Then, as described in the Appendix, the total scattered field is assembled by integrating over the stack of discs. This approach is an elaboration of the procedure used by Kerr [1952] to calculate the scattering from metallic cylinders ignoring end effects. Kerr treats an isolated perfectly conducting finite cylinder of length h illuminated broadside ($\psi = 0$) by either vertically ($\vec{E}_V = E_V \hat{e}_z$) or horizontally ($\vec{E}_H = E_H \hat{e}_x$) polarized waves. The expressions given by Kerr for the cross sections are well known:

$$\sigma_V = \frac{4h^2}{\pi} \left| \sum_{n=0}^{\infty} (-1)^n (2 - \delta_{on}) \frac{J_n(ka)}{H_n(ka)} \right|^2 \tag{1}$$

$$\sigma_H = \frac{4h^2}{\pi} \left| \sum_{n=0}^{\infty} (-1)^n (2 - \delta_{on}) \frac{J'_n(ka)}{H'_n(ka)} \right|^2 \tag{2}$$

where J_n is the ordinary Bessel function, H_n is the (outgoing wave) Hankel function, $k = 2\pi/\lambda$, and δ_{on} is the Kronecker delta. By the procedure described in the Appendix, a multipath factor is introduced to account for the reflecting surface, and an additional factor, D^2, accounts for the fact that the cylinder is made of water. With these modifications, (1) and (2) take the form:

$$\sigma_V = \frac{4D_V^2}{\pi} \left| \sum_{n=0}^{\infty} (-1)^n (2 - \delta_{on}) \frac{J_n(ka\cos\psi)}{H_n(ka\cos\psi)} \right|^2 \cdot h^2 \cdot |F^V(f, \psi, kh)|^2 \tag{3}$$

$$\sigma_H = \frac{4D_H^2}{\pi} \left| \sum_{n=0}^{\infty} (-1)^n (2 - \delta_{on}) \frac{J'_n(ka\cos\psi)}{H'_n(ka\cos\psi)} \right|^2 \cdot h^2 \cdot |F^H(f, \psi, kh)|^2 \tag{4}$$

where $F^{V,H}$ depends on the complex reflection coefficients for the water surface and is given in (A5), and $D_{V,H}^2$ are empirical factors. A further assumption required in the conversion of (1) and (2) into (3) and (4) is that at the disc surfaces, the exterior boundary conditions for a highly reflective surface "resemble" those for a perfectly conducting surface. Solutions for a dielectric cylinder [see King and Wu, 1959, Chapt. 2] would indicate that this is a good assumption for thin water cylinders. Moreover, in comparing the backscatter cross sections of metal and water spheres, Aden [King and Wu, *loc. cit.*] found that the scattering behavior versus ka was virtually the same, both theoretically and

experimentally, only the mean cross section level for the water spheres was about half that for the metal spheres. This result supports our "resemblance" assumption, and suggests a value of about 0.5 for the empirical factor D^2. (The reflection coefficient of a plane water surface is about 0.75 at microwave frequencies, further supporting this choice.) The wall of the "crown" is seen to be quite thin in some of the photographs, so we might be concerned whether a solid-post model is suitable for this structure. However, calculations of the reflection coefficient for a thin sheet of water [see Stratton, 1941, p. 515] indicate that at X-band, at least, the reflection coefficient remains quite high for thicknesses down to about 0.25mm, which is certainly very thin.

The cross sections can be expressed more compactly by letting $(4/\pi)$ times the respective sum terms in (3) and (4) be denoted by the symbol $C^{V,H}$, putting $D^2 = (1/2)$, and writing

$$\sigma_{V,H}\,(a,h;f;\psi) = (1/2)\,C^{V,H}\,(ka\cos\psi)\cdot h^2\cdot\,|\,F^{V,H}\,(f,\psi;kh)\,|^2 \qquad (5)$$

where the dependence on cylinder radius, a, height, h, and illuminating frequency, f, and grazing angle ψ, is made explicit. The cylindrical scattering factors $C^{V,H}$ were computed from their eigenfunction expansions, with the results shown in Fig. 8. The multipath factor $F^{V,H}$ depends on frequency through both kh and the complex reflection coefficient $R_V(f,\psi)$; for horizontal polarization, $R_H \approx -1$ for almost all frequencies at relatively low grazing angles. The factors $|F^{V,H}|^2$ are plotted in Fig. 9 for sea water, using the amplitude and phase of R_V at 3 cm. (X-band) given in Saxton and Lane [1955].

A. Application of the Metallic Cylinder Model:

We will begin by applying the simple scattering model outlined above to the crown and stalk phases of a splash event characterized by the parameters of the particular measurement recorded in Fig. 6a: X-band radar (10 Ghz) viewing the splash of a 4 mm drop at a grazing angle of 15°. It will be necessary to make certain assumptions about the dimensions and time behavior of the splash structures. Both crown and stalk will be assumed to rise and fall linearly over their lifetimes, the crown lasting 50 msec and rising to a maximum height of 1D (4mm) with a mean diameter of 3D (12mm), while the stalk lasts 150msec, rising to 6D (24mm) with a diameter of (3/4)D (3mm). Thus in Eqn. (5) the crown will have $ka_c = 1.3$ with a maximum $kh_c = 0.8$, and the stalk $ka_s = 0.3$ with a maximum $kh_s = 5$. The resulting time histories of the crown and stalk cross sections are plotted in Fig. 10 for both horizontal and vertical polarizations. For scaling, we have shown the return from a 4mm spherical water drop as it would be seen at the peaks of the interference pattern above the surface for both polarizations (V-Pol line at -14dBcm^2; H-Pol at -7dBcm^2). Their difference is due to the different surface reflection coefficients for the two polarizations.

In comparing the model predictions in Fig. 10 with the actual measurements in Fig. 6, the almost total disagreement for the vertically polarized stalk returns is most striking. But there are also some strong similarities that become clearer if Fig. 10 is plotted against the same linear power scale that was used in Fig. 6. This is done in Fig. 11a, using the peak of the vertical crown return as a reference for comparison with the first 200msec of the experimental curve sketched below it (Fig. 11b, sketched from Fig. 6a.) The small returns on the left in the experimental records are ascribed by Hansen to the passage of the bare drop through the interference pattern above the surface before it strikes, so these levels should correspond to the "bare drop" cross sections given in Fig. 10. Bare-drop returns are simulated on Fig. 11a by short vertical lines at the approximate locations one would expect them to occur relative to the splash process. There is a bit of ambiguity in properly identifying the small pips in this part of the records (for example, Hansen has suggested that the right-hand pip on the H-pol record might be the crown return), but if they could, indeed, be validated as bare-drop returns the measurement would become self-calibrating, since the cross section of a water sphere of given diameter is rather precisely known. However, if we accept all of the assumptions made thus

far, we would conclude from Fig. 11 that the simple "metallic cylinder" model is in surprising agreement (within a few dB) with the measured behavior of Crown scattering and Horizontal Stalk scattering, but fails to account for the sharp cut-off and oscillating behavior of the Vertical Stalk return. Obviously, for these large splashes, there is something seriously wrong with the assumptions underlying our cylindrical scattering model for vertical polarization.

B. A Dielectric Waveguide Model of the Stalk:

In applying the metallic cylinder model, the basic assumptions are that the scattered field components just outside the surface of the cylinder are uniform in the axial direction, that there are neither interior fields nor end effects, and that the aqueous nature of the cylinder is accounted for by the empirical factor $D^2=0.5$. However, dielectric cylinders can support a variety of internal waveguide modes, and if these were excited by an incident wave one might expect some interesting scattering behavior. Figure 12a shows the field configurations in a dielectric rod for the first (lowest) two waveguide modes: TM_{01} and TE_{01}. The cut-off frequencies for both modes are given by

$$f_c = 11.5/\sqrt{(K-1)}a \quad \text{GHz}. \tag{6}$$

where K is the dielectric constant of the rod and a is its radius in cm. [see Jackson, 1962, or Johnson, 1965]. For water at X-band frequencies, K = 60, so the cut-off frequency for a 3mm stalk diameter is 9.9 Ghz. Although we will not hold these formulas to exact applicability, it is comforting that the cut-off frequency lies in the right range.

While the TE_{01} fields would be very difficult to excite with an external plane wave, the magnetic field in the TM_{01} mode is a simple elaboration of the field in the metallic cylinder model. This is illustrated in Fig. 12b where the magnetic field circling the rod at the right is uniform along the rod, while that belonging to the TM_{01} mode on the left has the same symmetry, but changes direction along the rod with the periodicity of the wavelength in the rod. This wavelength is obtained from the dispersion diagram for the mode, shown in Fig. 13 (based on Johnson, 1965, Fig. 4.45).

In order to explore the implications of this idea, we must imagine that somehow the vertically polarized incident wave excites a TM_{01} mode as a standing wave in the growing stalk. The azimuthal magnetic field in this mode is continuous across the surface, and enters the scattering integral in (A1) to become the source of the scattered field. We see in Fig. 14a that as the stalk grows from zero, the polarity of the magnetic field changes with each half-wavelength of stalk length. This phase dependence, when added to that produced by oblique incidence and the grazing angle dependence of the surface reflection coefficient, could give rise to a scattered field of considerable complexity. Without attempting an actual solution of the dielectric rod problem, we will simulate the axial behavior of the surface magnetic field by inserting a factor with the right periodicity into the integrand of (A1). A cosine function is chosen to ensure that the electric field at the base of the rod will be tangential to the rod surface, resulting in the substitution:

$$H(r') \rightarrow H(r') \cos(k_g z'), \tag{7}$$

where k_g is the wavenumber in the dielectric rod, as given by the dispersion curve in Fig. 13. This cosine factor now appears under the integral in (A3), with the integrated expression resembling (A5) but having twice as many terms. In order to determine the value to use for k_g, we return to the cut-off relation (6). As noted, the cut-off frequency for a 3mm diameter water rod is at X-band, so we expect the guide wavelength to differ very little from the free-space wavelength at the measurement frequency. Using the cosine from (7) in (A3) with $k_g = k_0$, and performing the integral to find the equivalent of (A5) for the dielectric rod problem, we obtain, finally, the scattering behavior plotted in Fig. 14b for the 15° grazing angle used in the experiment. The experimental profile is sketched to the

same scale to compare the time histories (quantitatively it turns out to be about twice the predicted value.) Clearly, the dielectric rod model looks promising as an explanation for the peculiar behavior of the vertically polarized splash.

Additional support for this hypothesis is found in some measurements being made by Hansen (private communication) in which the equipment used to obtain the records shown in Figs. 5 and 6 measured the backscatter from a vertical water column contained in a plastic tube. By recording the time history of the scattered signal as the water was drained rapidly from the tube, the scattering behavior of a growing (or decaying) "stalk" was simulated. An example is shown in Fig. 14'a for a 9cm column with a diameter of 6mm, illuminated at a grazing angle of 27°. In Fig. 14'b the corresponding theoretical result, based on using (7) in (A3), is plotted for $k_g = k_a$. While the similarity of the two curves is striking, there are problems in both the experiment (a water film is left inside the plastic tube during the brief 300msec draining time), and the theory (the mode structure in the water column would be complicated by the plastic sleeve supporting it; in fact, it was necessary to use the free space wavelength in the rod to obtain the agreement shown, even though the guide wavelength for the 6mm column would have been much shorter). Nevertheless, the agreement shown in Figs. 14 and 14' certainly enhances the plausibility of the model.

The asymmetries in the scattering profiles for the falling drops are probably due, at least in part, to a difference between the growth and decay times for the stalk: the water column must labor to push itself upward against the forces of gravity and surface tension, and once having used up the energy available from the falling raindrop, it "crashes" in a much shorter interval (sometimes breaking up in the process, as in Fig. 3). The displacement of the central peak in Fig. 14b and the rounded leading edge in the H-pol return in Fig. 6 give evidence of this type of asymmetry. There are several other features in the experimental records that require explanation. The large return at about 260 msec in the V-pol record of Fig. 6a (see also Fig. 5) is associated with a secondary stalk formed by the "crash" of the main stalk. Although these secondary stalks can be quite tall, they are observed to be very thin. Thus their cut-off frequency would be much too high for dielectric-rod scattering, and they would probably scatter in the "metallic cylinder" mode. In fact, this V-pol return closely resembles the metallic cylinder H-pol return in the figure below it. Moreover, Hansen's preliminary measurements of scattering by water columns showed a thinner column of the same height as that in Fig. 14'a to scatter more strongly than the fatter column, and to display greatly reduced oscillations during its decay.

The small equally spaced returns marching off to the right are produced by interference between the advancing and receding edges of the "ring wave," as we will find in the next section. The 3mm stalk in Fig. 6b could be viewed as a variant of the 4mm case, or something quite different. We have seen the similarities between two different 4mm drops in Figs. 5 and 6a, but we have no additional data on the 3mm drop.

While one cannot avoid feeling at this point that scattering from the crown and stalk phases of the raindrop splash is fairly well understood, at least qualitatively, confidence in numerical cross section predictions will have to wait until measurements of splash scattering are available for a wider range of drop sizes.

V. SCATTERING BY THE RING WAVE

As mentioned earlier, the "Ring Wave" is a fugitive event, appearing a fraction of a second after impact and carrying away a portion of the energy of the fallen raindrop. In this sense, the splash process may be viewed as an intermediary for converting the kinetic energy of rain into the energy of capillary water waves covering the surface, although a rough calculation shows that only a small part is carried away in the ring waves. The characteristics of the individual Ring Waves may best be

determined by high-speed photography, or what is almost as good, by using a video camera. Figure 15 is a sample of a frame-by-frame video record of natural rain falling on a water surface [Cavaleri, 1985-86]. The ring waves are seen to stabilize quickly into a simple, well-defined shape that is retained even as the waves pass through each other. This is one of the properties often ascribed to a Soliton, although any linear wave group should also display this interpenetrability.

A. Characteristics of the Ring Wave:

Although of very low resolution compared to photographs, the video frames in Fig. 15 contain a surprisingly large amount of information. The wave shape, and hence its peaks and troughs, can be inferred from the shadowy relief. The maximum stalk height provides a rough yardstick for measuring lengths, while the video frame rate of one frame per 17 msec is the tick of the clock. Using these measures, we should be able to obtain estimates of the waveform, amplitude and velocity of the ring waves. Six sequences of the type shown in Fig. 15 were analyzed in the manner of Fig. 16. The initial wave peak emerges with the collapse of the crown in frame 3. The stalk reaches its maximum height in frame 5, and as it collapses it produces the second ring wave peak in frame 7. In this sequence we see a second stalk rising and collapsing in frames 9-13, giving rise to a weak secondary ring wave starting in frame 13. (We have ignored the considerably weaker parasitic capillaries that preceed the initial ring wave component.) All of the sequences analyzed looked the same, although not all displayed the "second splash." The dashed lines trace the propagation of the wave peaks, and their slopes give the wave velocity. Rough observation indicated that the maximum stalk heights were of the order of 1 inch, or about 2.5cm. Using this value to scale the radius of the expanding ring wave, the velocities were of the order of 25 cm/sec, which is close to the minimum of the velocity/wavelength characteristic for water waves (the transition between gravity and capillary waves.) The basic waveform produced by the sequential collapse of crown and stalk consists of two peaks separated by a trough. Applying the scale used to obtain the wave velocity, the two peaks appear to be separated by about 1.5-2.0 cm, which lies, again, at the minumum of the velocity/wavelength characteristic for water waves. This is reassuring, because it is just the kind of natural response that one would expect for an impulsive excitation of this type.

The waveform will be approximated by a circular wave traveling with velocity V and having the profile of a double- Gaussian of the form

$$\xi(\rho,t) = a\left(\frac{\rho_o}{\rho}\right)^{1/2}\left[e^{-\frac{(\rho-Vt)^2}{A^2}} - Ce^{-\frac{(\rho-Vt)^2}{B^2}}\right] \tag{8}$$

where ρ_o is a reference radius, and the parameters A, B, and C are chosen to provide a zero-mean water waveform, which requires that C = A/B. The cross-sectional contour of such a waveform with peaks separated by 2 cm is shown in Fig. 17, and seems to reflect rather well the general impression of the relatively deep trough separating the two peaks. For this particular waveform, A = 1cm, B = .65cm, and C = 1.54; we will use these values in the numerical example below.

B. A Perturbation Theory of Ring Wave Scattering:

It is obvious from the Figures that the amplitude of the ring wave can be at most a millimeter or so, making this one of the few scattering features on a water surface to which a perturbation approximation may legitimately be applied at microwave frequencies. We will use Wright's expression [1966] for scattering from a surface perturbation when $ka << 1$ (a is the maximum height of the perturbation):

$$\sigma_0(\theta) = \frac{4}{\pi}k^4 a^2 g_{VV}(\theta)\left|\int_S\int \zeta(x,y)e^{-2ik(x\sin\theta)}dxdy\right|^2 \tag{9}$$

where the angle factors $|g_{V,H}|^2$ are given by Valenzuela [1978], and plotted here in Fig. 18 for water at X-band frequencies. For the circularly symmetric perturbation in (8), the surface integral in (9) becomes the Hankel Transform of the ring wave perturbation, and, as shown in the Appendix, the cross section given in (9) takes the form given in (A16):

$$\sigma(t) = 32\pi k^4 a^2 |g_{V,H}|^2 \left(\frac{\rho_o}{\alpha}\right) A^2 \left[e^{-\frac{1}{4}(\alpha A)^2} - e^{-\frac{1}{4}(\alpha B)^2}\right] \sin^2(\alpha V t + \pi/4). \qquad (10)$$

Some typical values for the ring wave parameters might be A=1 and B=.65 as used in Fig. 17, V=25cm/sec as inferred from Fig. 16, a=0.1cm at ρ_o=1cm, and $\alpha = 2k\cos\psi = 4$ for X-band illumination at 15°. Referring to Fig. 18, we see that for V-polarization, the g-factor is 0.63, so putting all this into (19), we find the ring wave cross section to be

$$\sigma(t) = 0.17\sin^2(100t + \pi/4)\,\text{cm}^2 \qquad (11)$$

This expression predicts a return that oscillates with a period of about 30 msec and with an amplitude about 6dB below the height of the V-pol crown return, which almost exactly describes the small, equally spaced returns to the right of the main stalk return in Fig. 6a. For horizontal polarization, the g-factor given in Fig. 18 is seen to be 20dB lower, so the ring wave scattering for this polarization would be well below the threshold of observation.

VI. PREDICTION OF THE RAIN-RATE DEPENDENCE OF SPLASH SCATTER

The scattering models developed above pretty well describe the scattering behavior displayed in the laboratory experiments, but in order to apply these models to real rain splashes we would have to know much more about the characteristics of such splashes and the distributions of their parameters than we do at the present time.

A. The Stalk-Height Distribution:

We know that in natural rain the drops vary in size according to a drop-size distribution, which is a function of rain rate. We have observed that the splash dimensions seem to scale, in some way, with the size of the impacting drop, so we might expect that the individual splash cross sections would also be distributed in the manner of a drop-size distribution. The stalk is clearly the most important scattering feature in the splash, and careful scaling of maximum stalk heights from video records of natural rain splashes for various rain rates [Cavaleri, 1986] have shown two cases in which the distribution of maximum stalk heights looks very much like a Laws-Parsons drop-size distribution. This may be seen by comparing the Cavaleri stalk-height distributions with the Laws-Parsons drop-size distributions [see, e.g., Ulaby, et al, 1981] for the same rain rate R, as is done in Fig. 19 for R=4mm/hr and R=6.4mm/hr. Such comparisons also yield an empirical estimate of a scale factor that can be used to convert drop sizes to splash dimensions. Note that the peaks of the two stalk-height distributions in Fig. 19 occur at h_o=.9cm and h_o=1.5cm, respectively, while the peaks of the corresponding drop-size distributions appear at D=1.3 and 1.7cm. The indicated scale factors h_o/D convert the lower curves into the distributions sketched onto the upper curves, thus establishing a relationship between maximum stalk heights and the size of the drops producing them. While individual "rains" can have unique drop-size distributions depending on meteorological conditions, the similarity of the stalk height and drop-size distributions in Fig. 19 suggests that the Laws-Parsons distribution $p_{LP}(D)$ might sometimes provide a reasonable estimate of the stalk height distribution $p(h_o)$. For such cases we would write

$$p(h_o, R) = p_{LP}[D(h_o), R]\,|dD/dh_o| \qquad (12)$$

B. The Effects of Surface Slopes:

In modeling the scattering from natural raindrop splashes on a real sea surface, we must make some assumption about the state of the surface. The laboratory measurements described earlier were made with the mirror-flat water surface of an indoor tank, so the local grazing angle could be put equal to the antenna depression angle. But such surfaces are quite unusual on open bodies of water, since there is usually a little wind somewhere on the surface leading to some local "swell" or "chop," even for "calm" conditions, and in estuarine waters like the Chesapeake Bay, there will be agitations due to the gradients of the tidal currents and to boating, both pleasure and commercial. And of course, the splashes themselves produce some measure of "microchop." For these reasons, the surface on which the raindrop splashes are produced will generally have a non-vanishing slope which must be taken into account in defining the local grazing angle in the scattering formulas.

The grazing angle enters the expression for the stalk cross section through the factors C and F in (5). In C it appears in a cosine, whose small variation from unity over the range of angles of interest here (2-15°) will be ignored. The function F, on the other hand, is a sensitive function of grazing angle, through both the $kh \sin\psi$ dependence of its trigonometric functions and the surface reflection coefficient for the vertically polarized case. The effect of surface slope on stalk cross section may therefore be calculated simply by replacing the $|F|^2$ factor in (5) by its average over the surface slope distribution p(s):

$$\overline{|F^{V,H}|^2} = \int_{-\psi_0}^{\infty} |F^{V,H}(\psi_0 + s)|^2 p(s) ds \tag{13}$$

where the lower limit corresponds to zero local grazing angle, below which the stalk would be in "shadow." Although we really do not know what slope distribution to expect under the conditions we are discussing, we probably will not go too far wrong by assuming it to be Gaussian, with rms value s_0. Figure 20 illustrates the result, calculated from (13), for a grazing angle of 2° and rms slopes of 0.01, 0.05, 0.10 and 0.15. Comparison with the corresponding curves for a 2° grazing angle in Fig. 9 shows how important the effects of slope can be, particularly for horizontal polarization (this was also found to be true in the case of sea scatter [see Wetzel, 1987]).

C. Calculating the Average Cross Section:

The instantaneous stalk cross section given in (5), with the F-factor replaced by the average (13), is a function of stalk radius a, stalk height h, mean grazing angle ψ_0 and radar frequency f. Both the radius a and the maximum stalk height h_0 are observed to scale with the drop diameter D, so it will be assumed that a is simply proportional to h_0. This means that the cross section in (5) may be considered to be a function of maximum stalk height h_0 and instantaneous stalk height h,

$$\sigma_s(h, h_0) = \frac{1}{2} C(h_0) \cdot h^2 \cdot \overline{|F^{V,H}(h)|^2} \tag{14}$$

where the dependence on ψ_0 and f is assumed. There are only two splash-related parameters, h and h_0, so if we let $p(h, h_0; R)dhdh_0$ be the probability for rain rate R that a stalk will have a maximum height between h_0 and $h_0 + dh_0$, and be observed at a height between h and $h + dh$, then the average cross section per stalk for rain rate R is written as

$$\sigma_s(R) = \int_0^{\infty} \int_0^{\infty} \sigma_s(h, h_0) p(h, h_0; R) dhdh_0 . \tag{15}$$

The problem, then, is to find the joint probability density $p(h, h_0; R)$.

In discussing the laboratory measurements of stalk scattering in section IV, we assumed that the stalk rose and fell linearly, although there was evidence that the stalk labored up to its maximum height, and then fell more quickly. However, if we again assume that the rise and fall is linear, then the distribution of stalk heights seen by the radar will be uniform, so the provisional probability that a stalk of maximum height h_o will be observed at a height h is just

$$p(h \mid h_o) = \begin{cases} 1/h_o, & h < h_o \\ 0, & h > h_o \end{cases} \tag{16}$$

and the joint probability becomes:

$$P(h, h_o; R) = p(h \mid h_o) p(h_o; R) = (1/h_o) p(h_o; R). \tag{17}$$

Using (14) and 817) in (15), the average cross section per stalk for rain rate R may be written in the form

$$\bar{\sigma}_s^{V,H}(R) = \int_0^\infty dh_o p(h_o; R) \mathcal{A}^{V,H}(h_o). \tag{18}$$

where all of the scattering behavior is contained in the function

$$\mathcal{A}^{V,H}(h_o) = \frac{1}{2h_o} C^{V,H}(h_o) \int_0^{h_o} dh \cdot h^2 \overline{|F^{V,H}(h)|^2} \tag{19}$$

By separating the integrand in this way, it becomes possible to examine the interaction between the scattering characteristics of the stalks and their size distributions. At the top of Fig. 21 we show a stalk height distribution $p(h_o)$ of the type found in Fig. 19, while below it the scattering functions $\mathcal{A}^{V,H}(h_o)$ are given for a mean surface slope $s_o = 0.1$ and a stalk diameter $2a = 0.1 h_o$. No account has been taken in the V-pol curve of the possibility of exciting the dielectric-waveguide modes discussed in section IV.B; the dashed line at -18 dB indicates the level associated with the onset of such a mode for a stalk height corresponding to a drop size of roughly 3mm.

Taking the average over the stalk height distribution according to (18), the average stalk cross sections for the 6.4mm/hr rain rate become

$$\bar{\sigma}_s^V = -48 \text{ dBm}^2, \quad \bar{\sigma}_s^H = -66 \text{ dBm}^2, \quad R = 6.4\text{mm/hr}, \tag{20a}$$

and doing the same thing for the other rain rate in Fig. 19, we obtain

$$\bar{\sigma}_s^V = -51 \text{ dBm}^2, \quad \bar{\sigma}_s^H = -75 \text{ dBm}^2, \quad R = 4.0\text{mm/hr}. \tag{20b}$$

This example illustrates what is already obvious in Fig. 21, the vertically polarized return is determined chiefly by the dominant bulge in the drop (stalk) size distribution, so is only weakly dependent on the rain rate, while the horizontally polarized return is most sensitive to the population of larger drops (stalks) in the tail of the distribution, and is thus sensitive to both the rain rate and the particular shape of the size distribution curve.

Finally, in order to convert mean cross sections per stalk into Normalized Radar Cross Sections (NRCS's) for stalk scattering in natural rain, we will need the *flux* of stalk production on the surface - i.e., the number of stalks per square meter per second produced on the surface, as a function of rain rate R. Although not every drop will produce a stalk, the flux of raindrops of all sizes on the surface is given in Ugai, et al, [1977] by the empirical expression

$$N_D(R) = 1920\, R^{0.71} \text{ drops/m}^2\text{-sec} \tag{21}$$

On the other hand, Cavaleri [1986] has measured the flux of stalk production by direct observation, and found that while the temporal behavior of the stalk flux will be different for different "rains," a reasonable value for rain rates of about 4mm/hr is $N_s \sim 400$ stalks/m^2-sec, which is less than a tenth of the total drop flux given by (21) for the same R. Whatever the correct expression turns out to be, the stalk flux must be multiplied by the stalk *lifetime* T_s to get the total number of stalks per square meter that will be scattering back to the radar at any instant. Thus the NRCS for stalk scattering becomes:

$$\text{NRCS}_s = \bar{\sigma}_s(R) N_s(R) T_s \quad \text{m}^2/\text{m}^2 \tag{22}$$

Unfortunately, there are as yet no measurements by which the predictions of this theory could be tested with any confidence. The measurements by Hansen several years ago [1984], shown here in Fig. 4, consisted of median (not mean) backscatter data from the first few minutes of a beginning rainfall. Moreover, it is unlikely that an equilibrium drop-size distribution would exist during such periods, so the kinds of statistical drop (or stalk) size distributions we have been discussing could not even be defined, much less parameterized, by such a number as rain rate R.

VII. SUMMARY AND CONCLUSIONS

As a natural scatterer, the raindrop splash has a strong appeal for the scattering phenomenologist. It has three simple, cylindrically symmetric parts—the crown, the stalk, and the ring wave. These parts appear separately in a well defined time sequence, and can be treated as isolated, non-interacting scatterers, following simple laws of growth and decay. The crown and stalk resemble circular cylinders closely enough that well established formalisms may be used to estimate their scattering behavior, and the ring wave constitutes one of the few natural surface events to which a perturbation theory may be applied with any confidence. Yet, laboratory investigations of splash scattering have disclosed unexpected features in the scattering behavior that can be explained only by invoking more sophisticated models of the scattering process.

When applied to the well-defined and reproducible structures of a laboratory splash, the scattering models developed in this report have tended to describe the observed scattering behavior quite well. Although calibration of the experimental returns was uncertain, the predicted cross sections appeared to be of the right order of magnitude. The speculative "dielectric waveguide" model of stalk scattering for vertical polarization provided a qualitative explanation for the most puzzling aspect of the laboratory measurements, but while there is some encouraging support for it in recent measurements, it can be considered little more than a provocative hypothesis without further experimental confirmation.

The major problems in applying these models to scattering by natural rain splashes on a real sea surface lie in obtaining realistic estimates of stalk heigtht distributions and determining the effects of real surface slopes on cross section predictions. Examining the behavior of the stalk scattering function against sample stalk height distributions leads to the conclusion that vertically polarized returns will be only weakly dependent on rain rate, while horizontally polarized returns will be sensitive to both rain rate and the details of the height distribution curve. Unfortunately, the measurements made thus far in natural rain lack the simultaneous "ground truth" essentially drop (or stalk height) distributions and surface slope spectra necessary for meaningful intercomparison between theory and experiment.

The accumulation of a body of experimental data that would directly settle the outstanding problems in splash scattering on a a natural water surface is likely to be expensive, time-consuming, and frustrating. However, the theory is really quite straight- forward and believable, so some fairly reasonable inferences could be made from improved laboratory studies involving smaller grazing angles, a wide assortment of drop sizes, impact velocities closer to normal terminal velocities, and a surface that could be agitated to produce the varying slopes of a natural surface. Stalk scattering via a "dielectric waveguide" mode could be investigated as a separate problem. Such information, coupled with an expanded library of measured stalk height distributions and fluxes versus rain rate, should provide a basis for an adequate, if yet somewhat incomplete, understanding of the problem of raindrop splash scattering from "calm" sea surfaces.

As mentioned in the Introduction, this Report takes only a first step toward understanding the larger problem of how rain affects scattering from the sea surface. Much work remains to be done in this challenging field.

REFERENCES

Cavaleri, V. (1985-1986), During this period Cavaleri made many photographic and video records of both natural and artificial splashes, as well as analyzing some of these records to obtain stalk height distributions. This work will be described in detail in a report presently in preparation by J.P.Hansen (1987, below).

Engel, O.G. (1966), "Crater depth in fluid impacts," J. Appl. Phys., **37**, 1798-1808.

Hansen, J.P. (1984), "High resolution radar backscatter from a rain disturbed sea surface," ISNR-84 Record, Oct. 22-24, Tokyo, Japan.

Hansen, J.P. (1986), "A system for performing ultra high resolution backscatter measurements of splashes," Proc. of the International Microwave Theory and Techniques Symposium, Baltimore, MD. June 2-6.

Hansen, J.P. (1987), "Experimental characterization of high resolution radar backscatter from rain splash," NRL Memo Report, (In preparation).

Jackson, J.D. (1962), *Classical Electrodynamics*, (John Wiley and Sons, Inc., New York), Chapt. 8.

Jayaratne, O.W. and B.J. Mason (1964), "The coalescence and bouncing of water drops at an air/water interface," Proc. Roy. Soc. A, **280**, 545-565.

Johnson, C.C. (1965), *Field and Wave Electrodynamics*, (McGraw-Hill Book Company, New York), Chapt. 4.

Kerr, D.E. (ed.) (1951), *Propagation of Short Radio Waves*, Chapt. 6, (McGraw-Hill, New York, N.Y.).

King, R.W.P. and T.T. Wu (1959), *The Scattering and Diffraction of Waves*, (Harvard University Press, Cambridge, Mass.)

Moore, R.K., Y.S. Yu, A.K. Fung, D. Kaneko, G.J. Dome, and R.E. Werp (1979), "Preliminary study of rain effects on radar scattering from water surfaces," IEEE J. Oceanic Engin., OE-4, 31-32.

Saxton, J.A., and J.A. Lane (1952), "Electrical properties of sea water," Wireless Engineer, **29**, 269-275.

Stratton, J.A. (1941), *Electromagnetic Theory*, (McGraw-Hill, New YOrk, NY).

Ugai, S., K. Kato, M. Nishijima and T. Kan (1977), "Characteristics of raindrop size and raindrop shape," Proceedings of URSI Commission F Open Symposium of 28 Apr-6 May, 1977, La Baule, France, pp. 225-230.

Ulaby, F.T., R.K. Moore and A.K. Fung (1981), *Microwave Remote Sensing*, Vol. 1, Chapt. 5, (Addison-Wesley Publishing Co., Reading, Mass.)

Valenzuela, G.R. (1978), "Theories for the interaction of electromagnetic and ocean waves-a review," Boundary-Layer Meteor., **13**, 61-85.

Wetzel, L.B. (1987), "Models for electromagnetic scattering from the sea at extremely low grazing angles," NRL Memo Report 6098, September 1987.

Worthington, A.M. (1963), *A Study of Splashes*, (The MacMillan Co., New York, N.Y.; reprint of 1908 Edition; original work reported in Proc. Roy. Soc. (London), **34**, 217, (1882)).

Wright, J.W. (1966), "Backscatter from capillary waves with application to sea clutter," IEEE Trans. Antennas Propagat., **AP-14**, 749-754.

APPENDIX

1. Derivation of the Multipath Factor $F^{V,H}$

In Fig. 7, the scattering cylinder is pictured as a stack of discs of thickness dz, each scattering as if it were a slice of an infinite cylinder of radius a. Formally, the scattered (magnetic) field may be written in the following integral form [Kerr,1951]:

$$\vec{H}^S(\vec{r}) = -ik \frac{e^{-ikR}}{4\pi R} \int_S \int (\hat{n}_o x \hat{n} x \vec{H}(\vec{r})) e^{ik\hat{n}_o \cdot \vec{r}'} dS' \tag{A1}$$

where $\hat{n}_o$ is the direction to the observer and $\hat{n}x\vec{H}(\vec{r}')$ is the tangential component of the total magnetic field at the surface of the cylinder, and is proportional to the incident field at the point $\vec{r}'$ and to one or the other of the eigenfunction expansions in (1), (2). These two factors can be separated by writing

$$(\hat{n}_o x \hat{n} x \vec{H}) = (\hat{n}_o x \hat{n} x \vec{H}_o) H_{inc}(z) \tag{A2}$$

where H_{inc} is the combination of direct and surface-reflected fields at the height z, and H_o contains the eigenfunction expansion. For monostatic radar, the scattered field returns to the source over the same two paths that delivered the incident field to the disc, the two directions defining different $\hat{n}_o$'s in (A1). Although we could go through the formal manipulations via (A1), it easier and clearer to recognize that there are four possible ways a given disc can interact with the radar: direct ray incident, reflected ray incident, scattering into direct and surface reflected rays in both cases. Let $P_{i,j}$ denote the phases relative to the reference plane RP in figure (A1), where 1=direct ray, 2=reflected ray, and RP is defined by the grazing angle ψ and maximum cylinder height h.

The total scattered field is obtained from two integrals of the form of (A1), where only the phase factors remain inside the integral and all of the remaining factors are contained in the expression $H(k, a, \psi; R)$ (verification is left as an exercise for the reader):

$$H^S_{TOTAL} = H(k, a, \psi; R) \int_0^h [e^{iP_{11}} + Re^{iP_{12}} + Re^{iP_{21}} + R^2 e^{iP_{22}}] dz \tag{A3}$$

$R(\psi, f)$ is the (complex) reflection coefficient for water at frequency f and grazing angle ψ, and can be found in Saxton and Lane [1955]. The phases are obtained from the Figure above, and take the form:

$$P_{11} = 2k(l_1^0 + (h - z)\sin\psi); \quad P_{22} = 2k(l_1^0 + (h + z)\sin\psi) \tag{A4}$$

$$P_{12} = P_{21} = 2k(l_1^0 + h\sin\psi).$$

The integrals are easily performed, to yield a factor:

$$hF(k, h, \psi) = h[e^{ikh\sin\psi} sinc(kh\sin\psi) + 2R \tag{A5}$$

$$+ R^2 e^{-ikh\sin\psi} sinc(kh\sin\psi)]$$

which is used in Eqns. (3) and (4) for the metallic cylinder cross sections.

2. Reduction of Scattering Integral for the Ring Wave

The scattering integral in Eqn. (9) is given in rectangular coordinates for a plane wave incident in the positive-x direction:

$$I(k\cos\psi;t) = \int_S \int \zeta(x,y,t)e^{i2k\cos\psi x}\,dxdy\,. \tag{A6}$$

The ring wave is circularly symmetric, so the integral can be transformed into circular coordinates with the substitutions:

$$\zeta(x,y;t) = \zeta(\rho;t)\;;\quad x = \rho\cos\theta,\quad y = \rho\sin\theta,\quad dxdy = \rho d\rho d\theta \tag{A7}$$

and written

$$I(k\cos\psi;t) = \int_0^\infty \zeta(\rho,t)\,[\int_0^{2\pi} e^{i2k\rho\cos\psi\cos\theta}d\theta]\,\rho d\rho \tag{A8}$$

$$= 2\pi\int_0^\infty \zeta(\rho;t)\,J_o(2k\rho\cos\psi)\rho d\rho$$

which is just 2π times the Hankel Transform of the ring wave perturbation. Substituting (8) into (A8) gives two terms of the form:

$$I_\Delta(k,\psi;t) = 2\pi a\,\rho_o^{1/2}\int_0^\infty e^{-\frac{(\rho-Vt)^2}{\Delta^2}}\,J_o(2k\rho\cos\psi)\,\rho^{1/2}d\rho \tag{A9}$$

where Δ corresponds to either A or B. The ring wave is not fully developed until it is at least a stalk height, or so, from the splash center, so at X-band frequencies the argument of J_o in (A9) will generally be much greater than unity over the range of radii that are important in ring wave scattering. This means that we can use the asymptotic approximation for the Bessel function:

$$J_o(\alpha\rho) \simeq \left(\frac{2}{\pi\alpha}\right)^{1/2}\rho^{-1/2}\sin(\alpha\rho+\pi/4) \tag{A10}$$

$$= \left(\frac{2}{\pi\alpha}\right)^{1/2}\rho^{1/2}\left(\frac{1}{2i}\right)[e^{i(\alpha\rho+\pi/4)} - e^{-i(\alpha\rho+\pi/4)}],$$

and

$$I_\Delta \simeq i\sqrt{2\pi}\,a\rho_o^{1/2}\alpha^{-1/2}\,[e^{i\pi/4}\int_0^\infty e^{-\frac{(\rho-Vt)^2}{\Delta^2}}e^{+i\alpha\rho}\,d\rho - e^{-i\pi/4}\int_0^\infty e^{-\frac{(\rho-Vt)^2}{\Delta^2}}e^{-i\alpha\rho}d\rho]. \tag{A11}$$

The plus and minus phases may be viewed as identifying contributions from the receding and approaching sides of the ring wave, respectively. Because of the gaussian factors, the contributions to the integrals occur from a narrow range of $\rho \sim Vt \pm \Delta$, so we introduce a new variable $u = \rho - Vt$, and write

$$\int_0^\infty e^{-\frac{(\rho - Vt)^2}{\Delta^2}} e^{\pm i\alpha\rho} = e^{\pm i\alpha Vt} \int_{-\infty}^{\infty} e^{-\frac{u^2}{\Delta^2}} e^{\pm i\alpha u}\, du\,. \tag{A12}$$

The integral of the RHS is a standard type:

$$\int_{-\infty}^{\infty} e^{-\frac{u^2}{\Delta^2}} e^{\pm i\alpha u}\, du = \Delta \sqrt{\pi}\, e^{-\frac{1}{4}(\alpha\Delta)^2} \tag{A13}$$

by which the individual integrals are reduced to

$$I_\Delta \approx 2\pi\sqrt{2}\, a \left(\frac{\rho_o}{\alpha}\right)^{1/2} \Delta\, e^{-\frac{1}{4}(\alpha\Delta)^2} \sin(\alpha Vt + \pi/4) \tag{A14}$$

and the scattering integral (A6) to

$$I = \sqrt{2}\,(2\pi a)(\rho_o/\alpha)^{1/2} \left[Ae^{-\frac{1}{4}(\alpha A)^2} - BCe^{-\frac{1}{4}(\alpha B)^2}\right] \sin(\alpha Vt + \pi/4). \tag{A15}$$

Substituting into the expression (9) for the ring wave cross section yields, finally,

$$\sigma(t) = 32\pi k^4 a^2 \left|g_{V,H}(\psi)\right|^2 (\rho_o/\alpha) A^2 \left[e^{-\frac{1}{4}(\alpha A)^2} - e^{-\frac{1}{4}(\alpha B)^2}\right]^2 \sin^2(\alpha Vt + \pi/4). \tag{A16}$$

SERIES I*a*

Water into water (40 cm. fall). Scale $\frac{1}{10}$

SERIES I*a*—(*continued*)

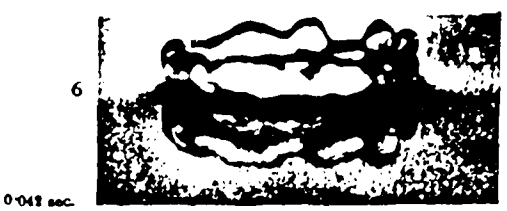

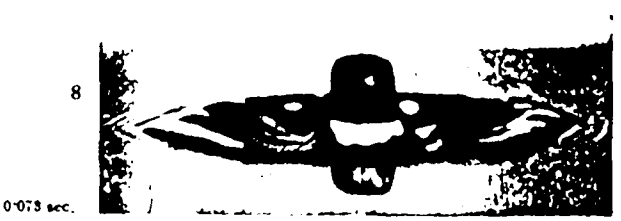

Fig. 1 — Samples of Worthington's Splash Photographs

SERIES Ia –*(continued)*

Running water. Scale reduced to $\frac{5}{6}$.

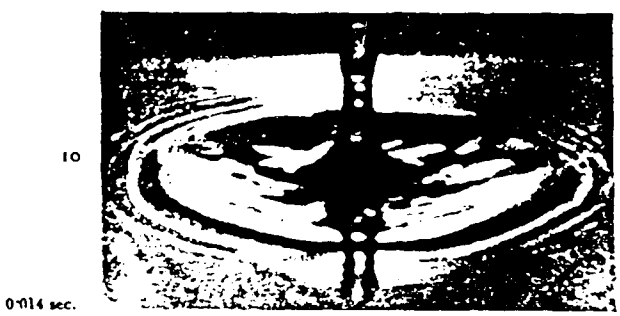

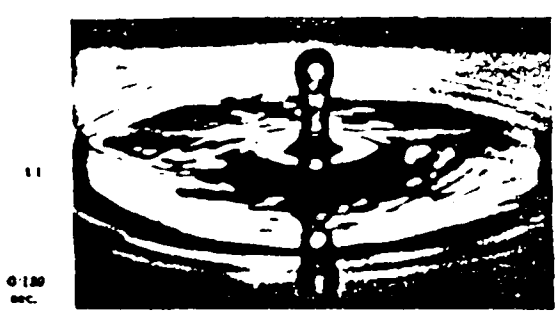

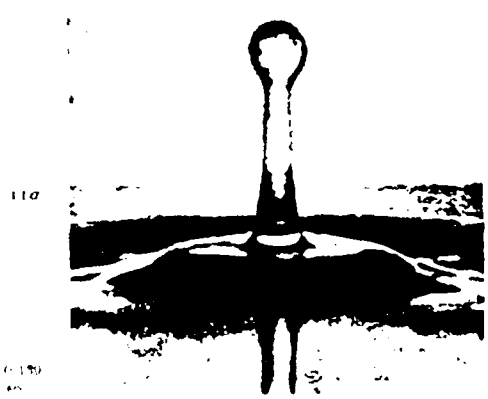

Fig. 1 (Continued) — Samples of Worthington's Splash Photographs

SERIES Ia—(*continued*)

Running water. Scale $\frac{6}{10}$.

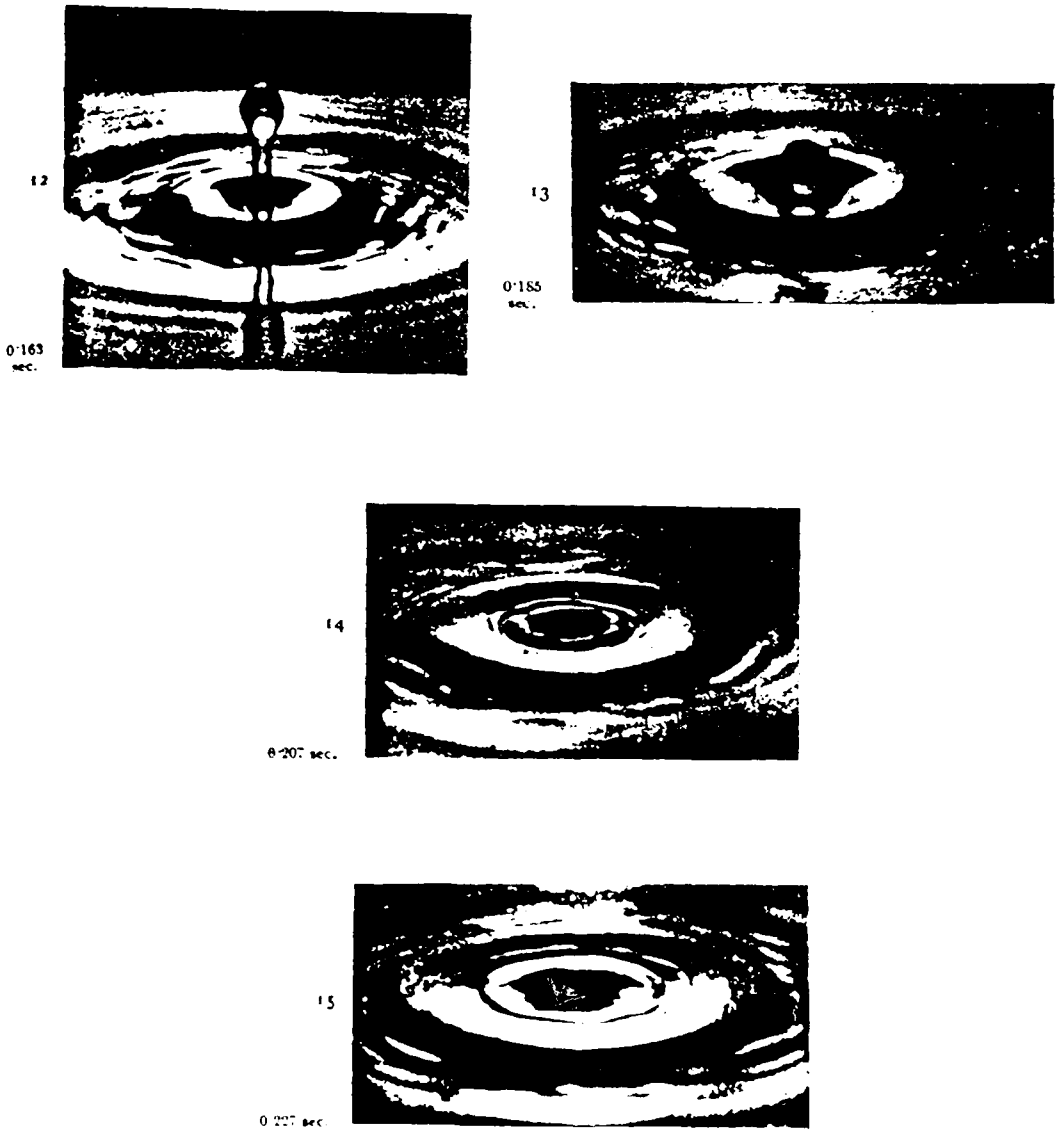

Fig. 1 (Continued) Samples of Worthington's Splash Photographs

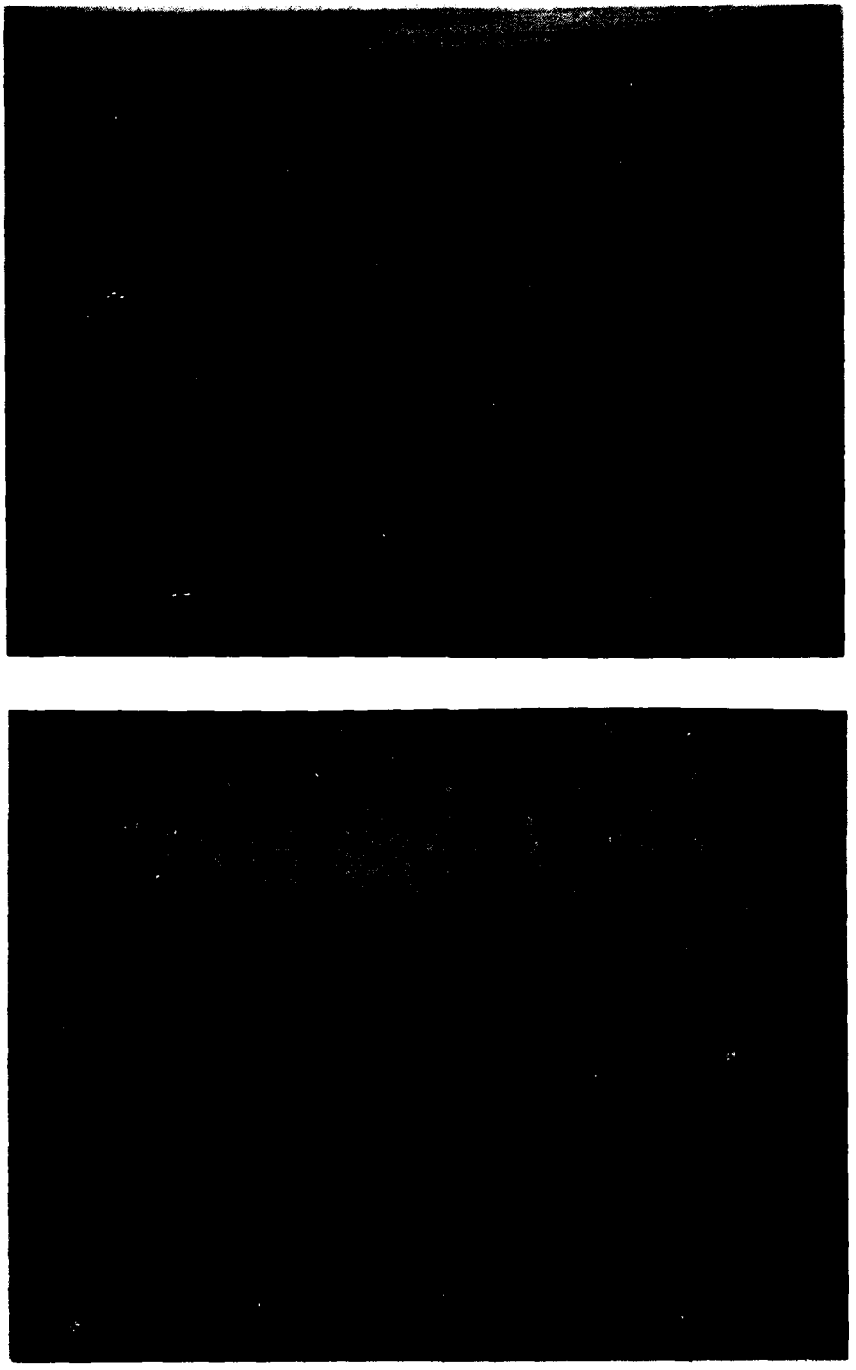

Fig. 2. Modern Splash Photographs (Cavaleri)

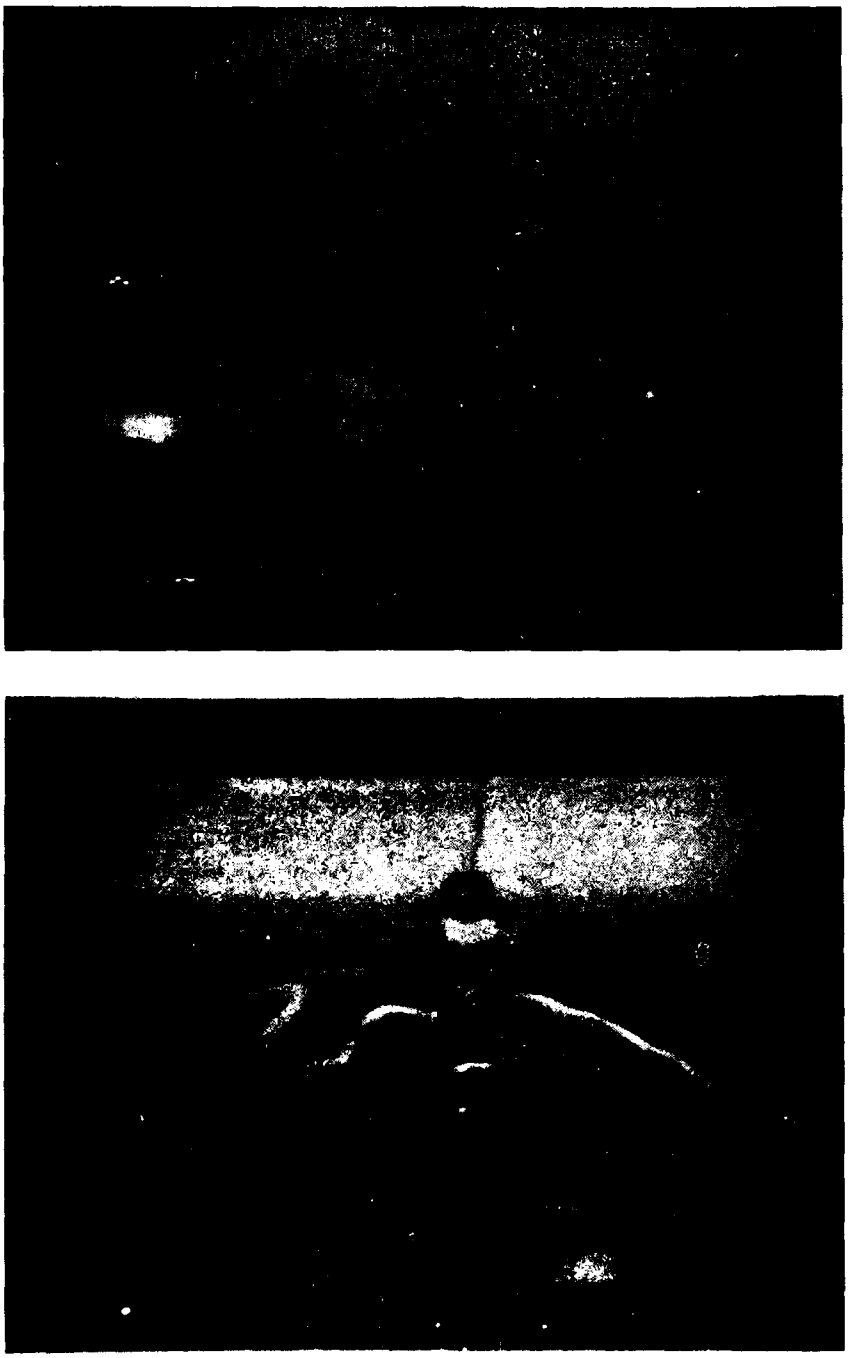

Fig. 2 (Continued) — Magnetic Resonance Photographs (Cavaleri)

WIND DISTORTION OF SPLASH FORMATIONS

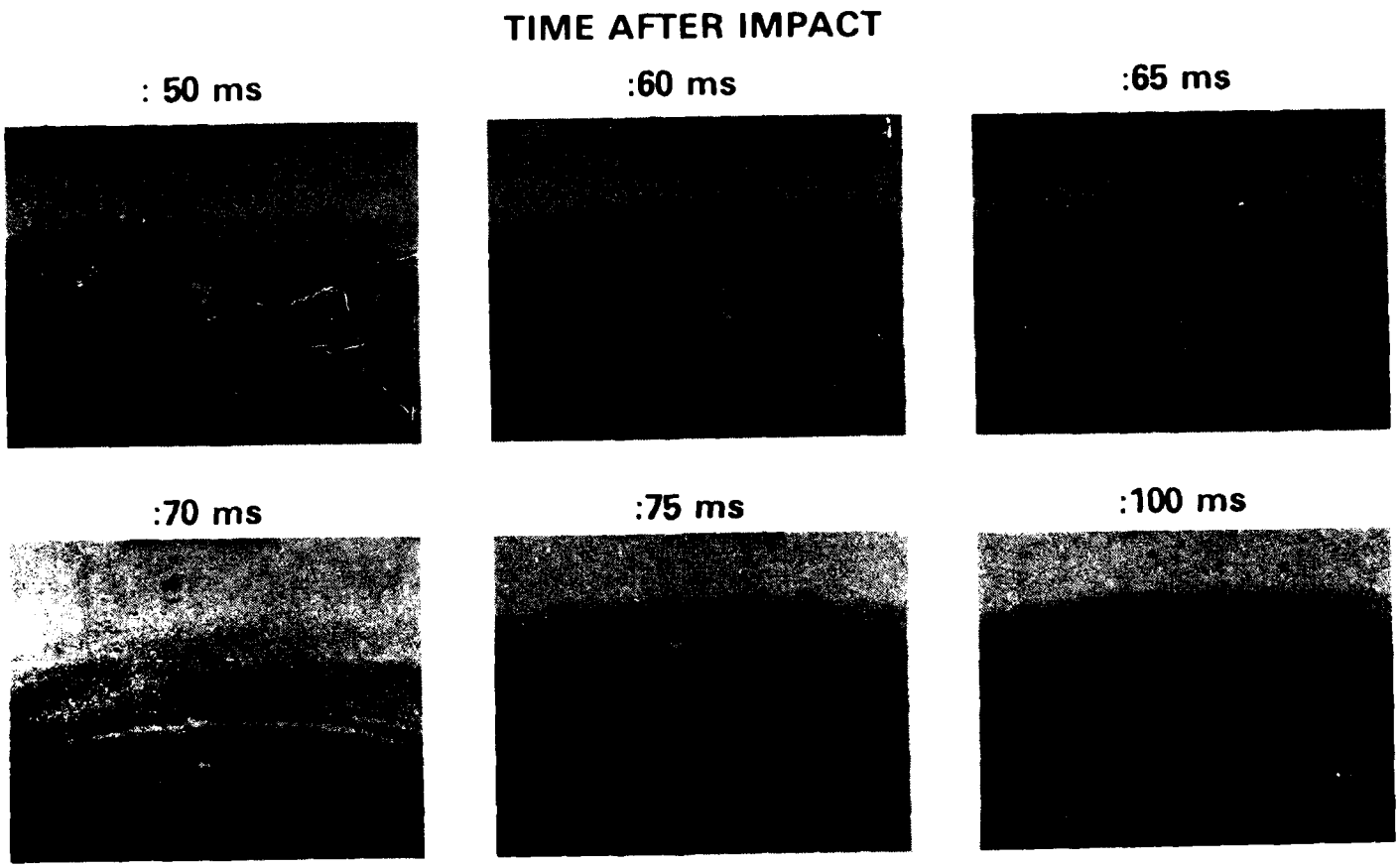

Fig. 3 — Separation of Droplets

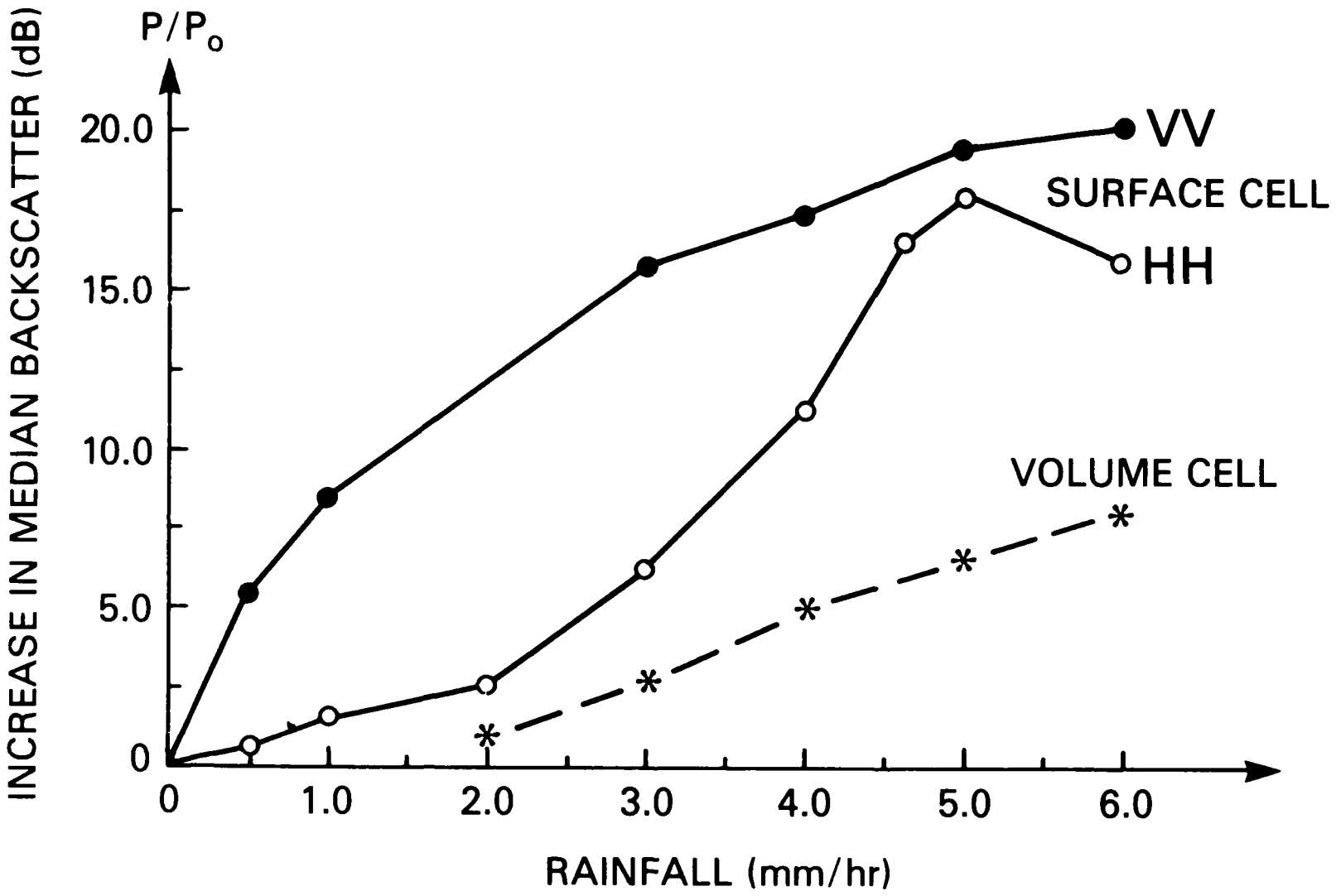

Fig. 4 — Rain Rate Dependence of Rain Backscatter from Calm Water

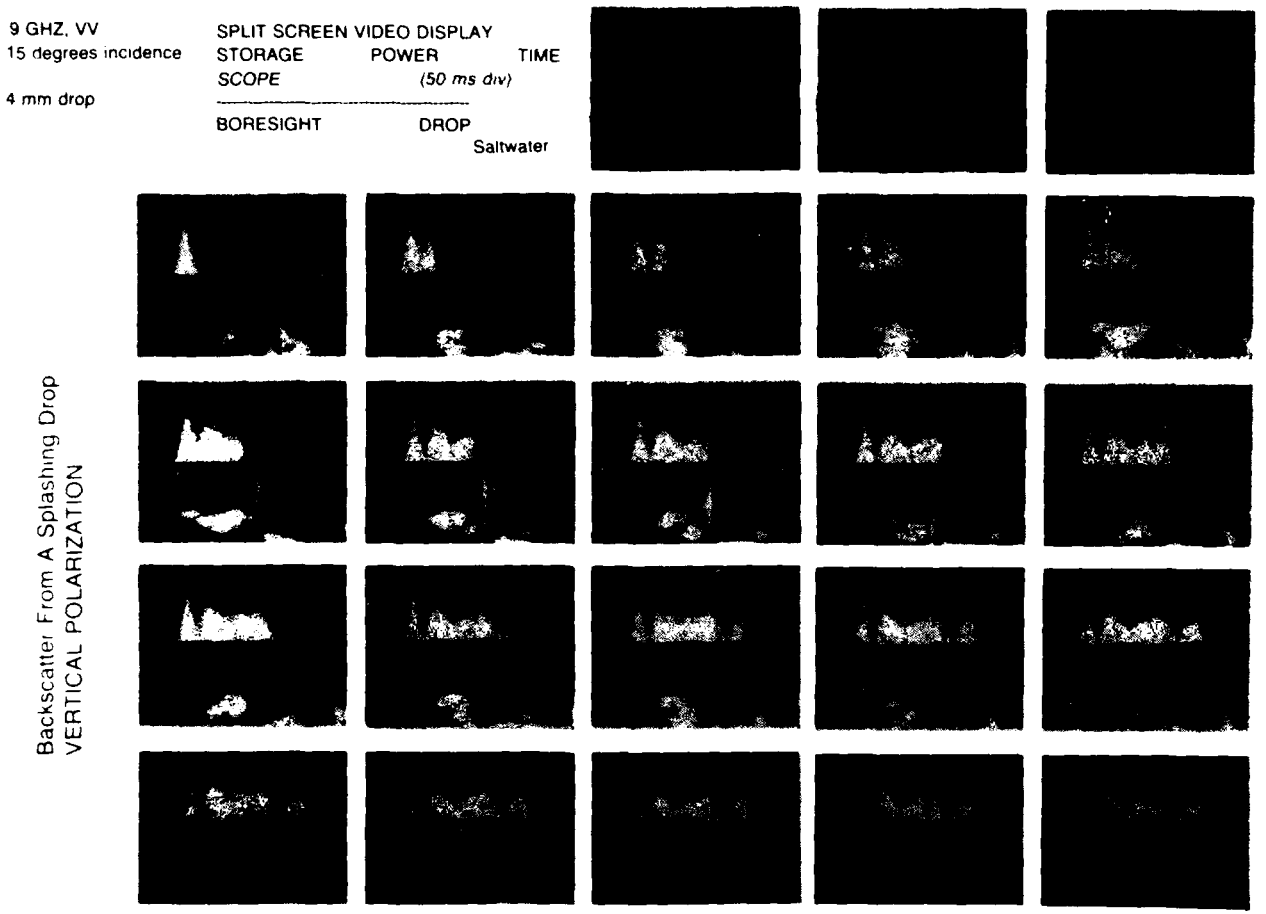

Fig. 5 — Time History of Backscatter from a Splash (V-Pol)

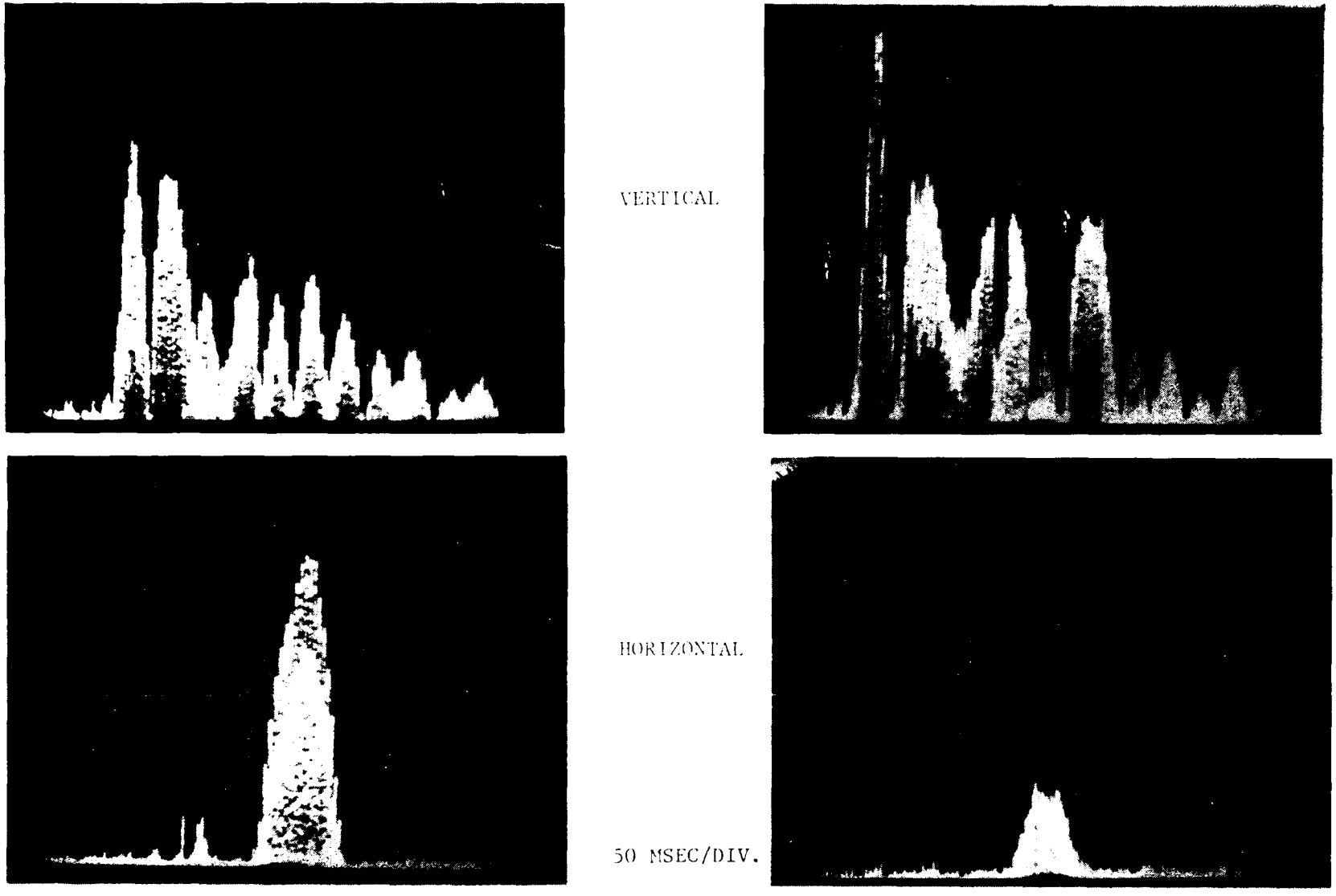

A. 4MM DROP

B. 3MM DROP

Fig. 6 — Comparison of V-Pol and H-Pol Returns versus Drop Size

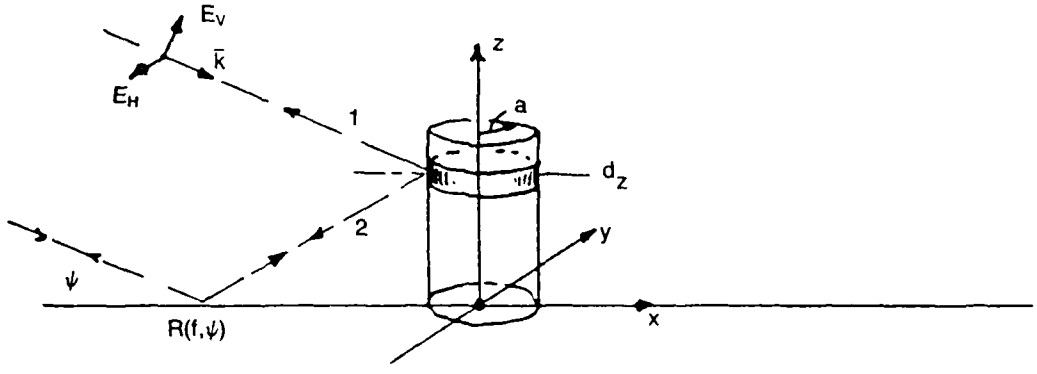

Fig. 7 — Scattering Geometry for the Cylindrical Crown/Stalk Model

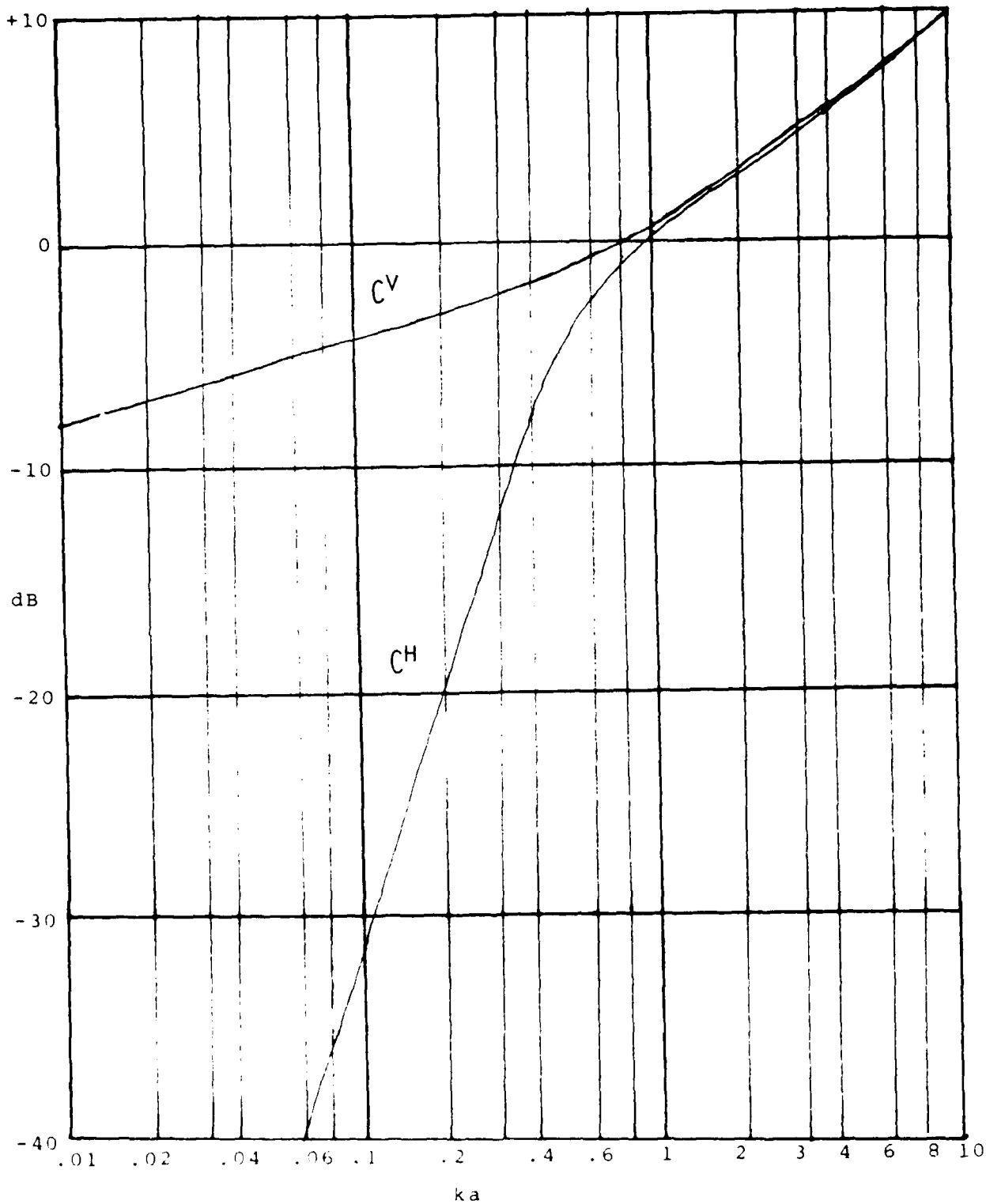

Fig. 8 – The Cylindrical Scattering Factors $C^{V,H}$

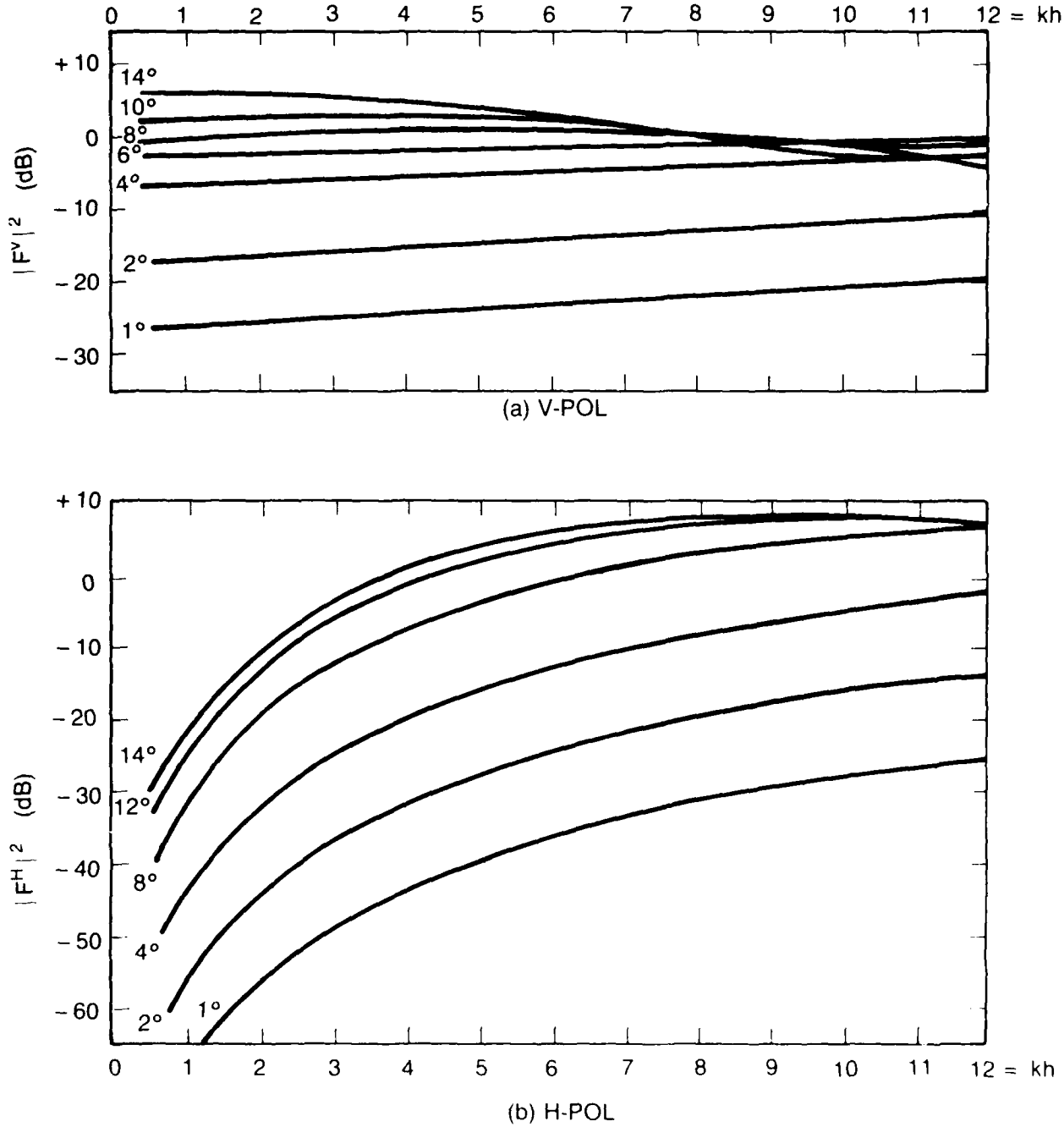

Fig. 9 — Multipath Factors $|F^{V,H}|^2$ versus kh and Grazing Angle

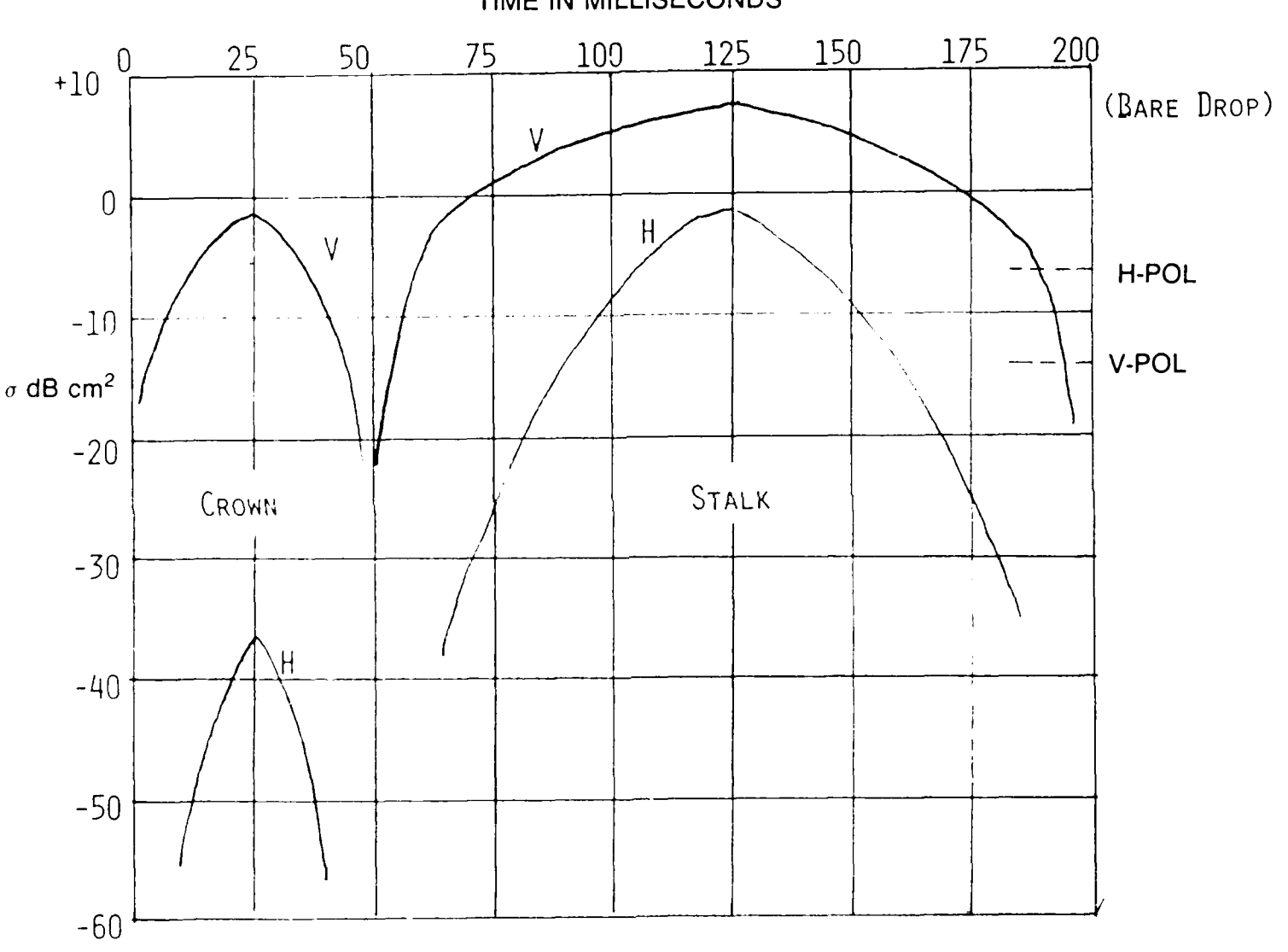

Fig. 10 — Crown and Stalk Cross Sections for Metallic Cylinder Model

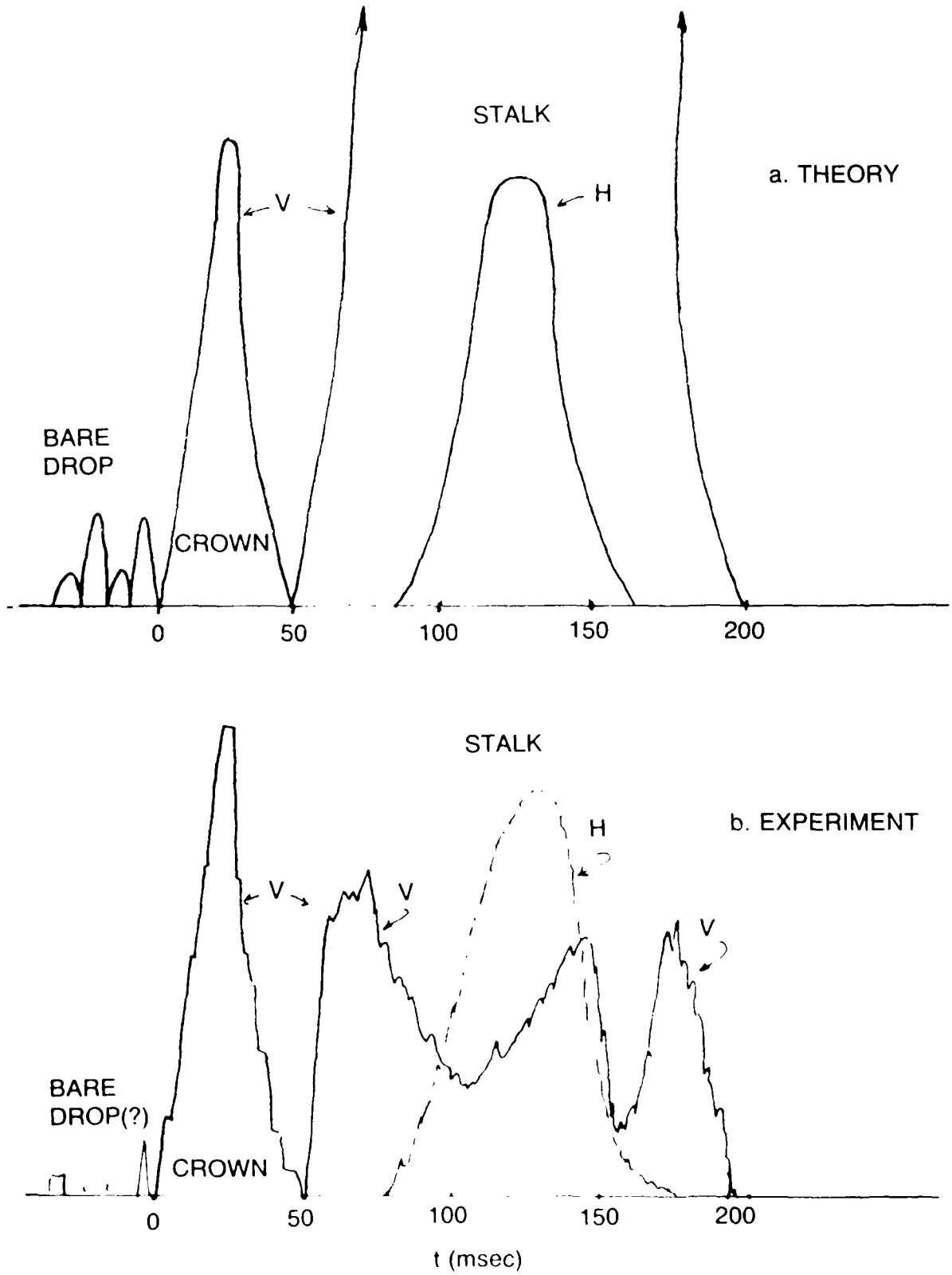

Fig. 11 Metallic Cylinder Model Compared with Measurements

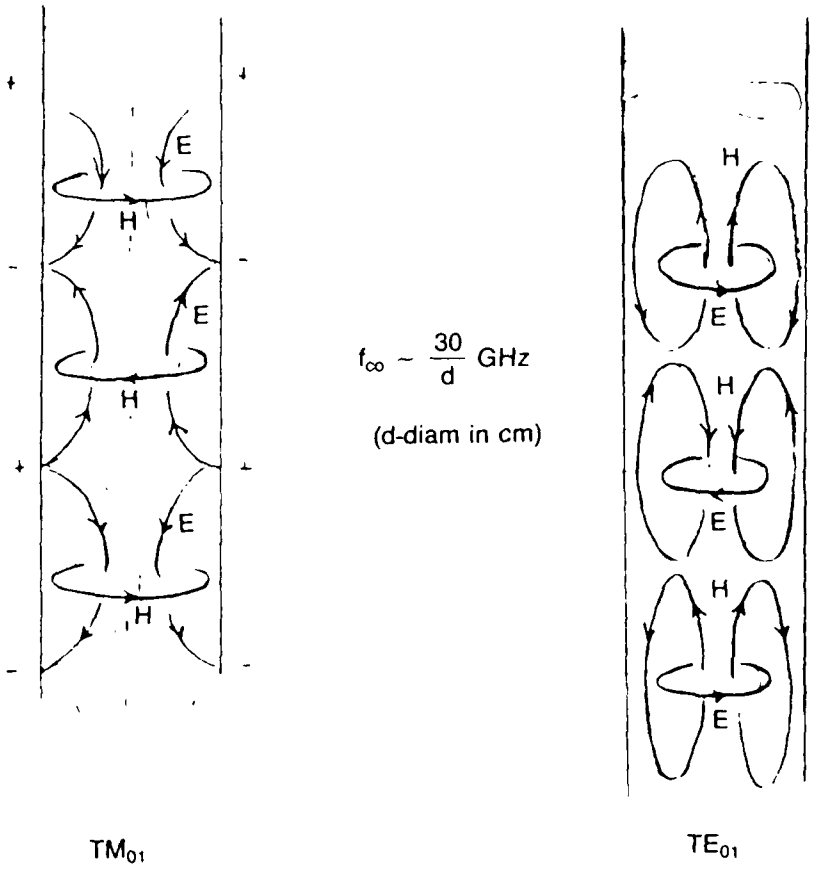

a. Interior fields in a dielectric rod

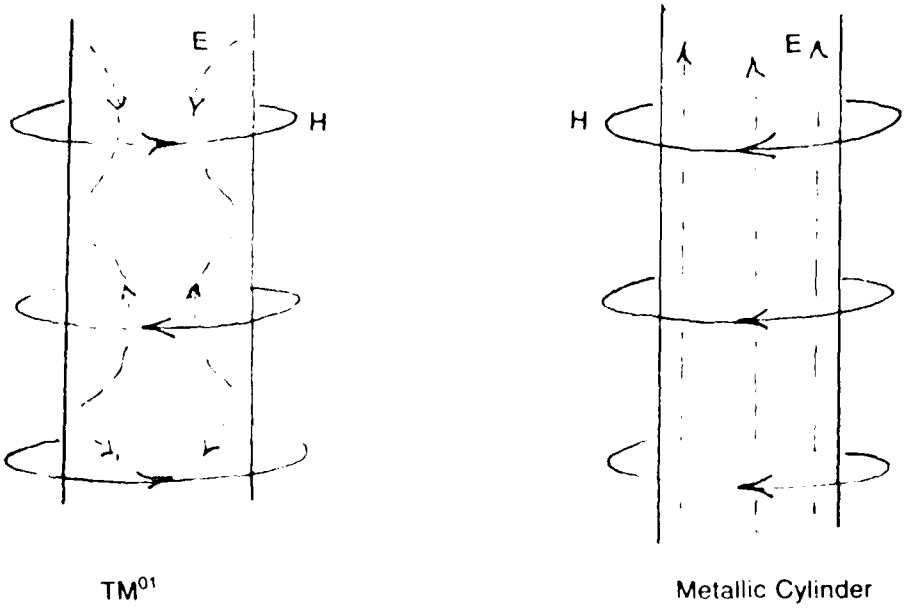

b. Exterior Magnetic Fields in dielectric and metal rods

Fig. 12 — Waveguide Modes in a Dielectric Rod

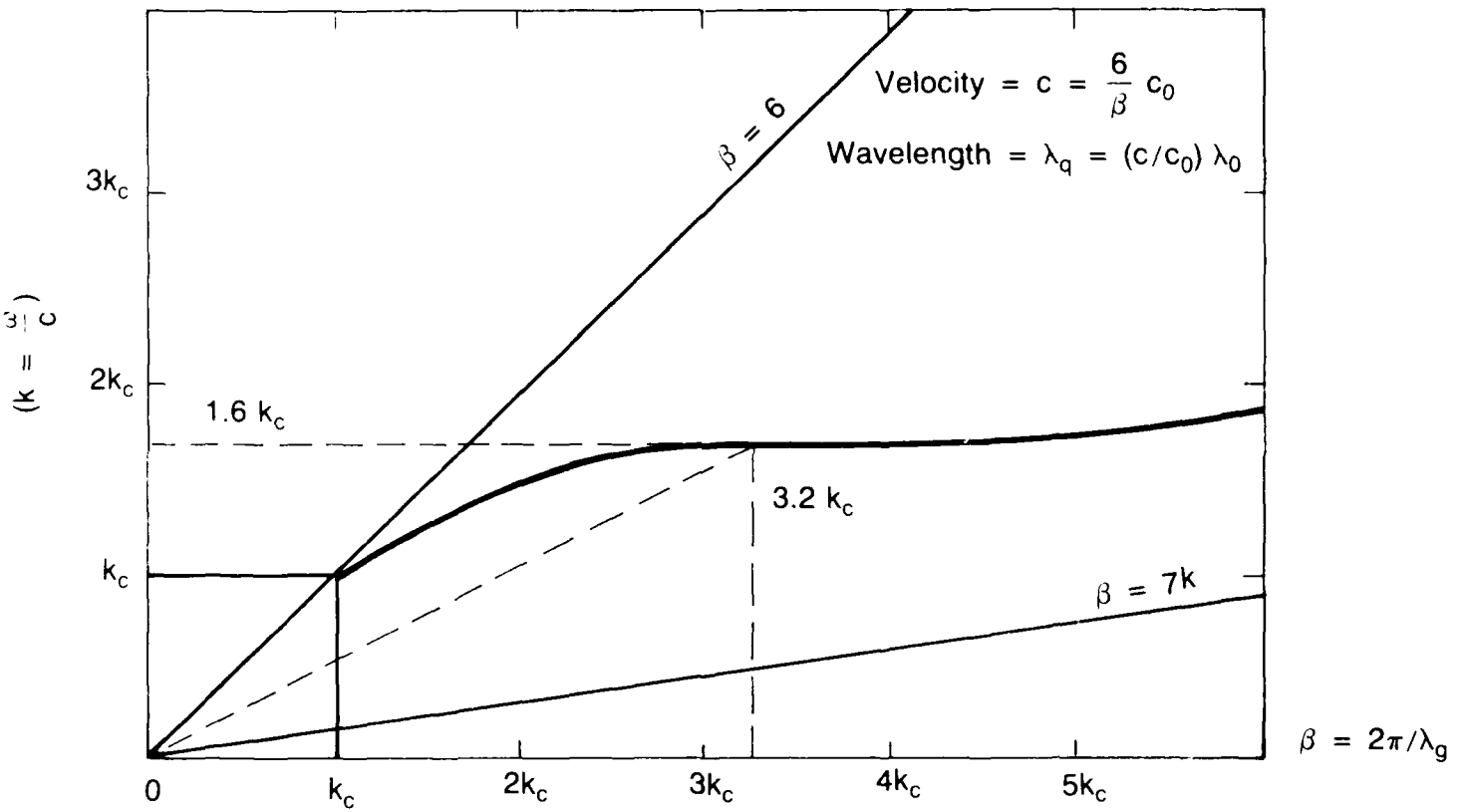

Fig. 13 — Dispersion Diagram for TM_{01} Mode, $\epsilon = 60$

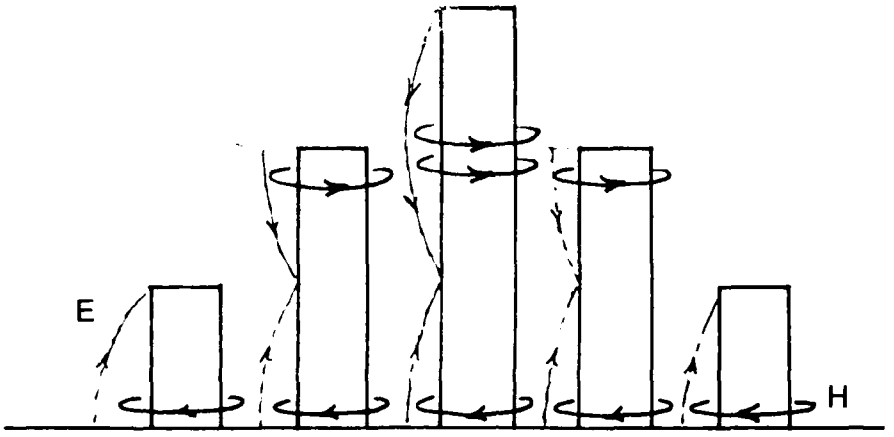

a. Changing Field Configurations with Changing Stalk Height

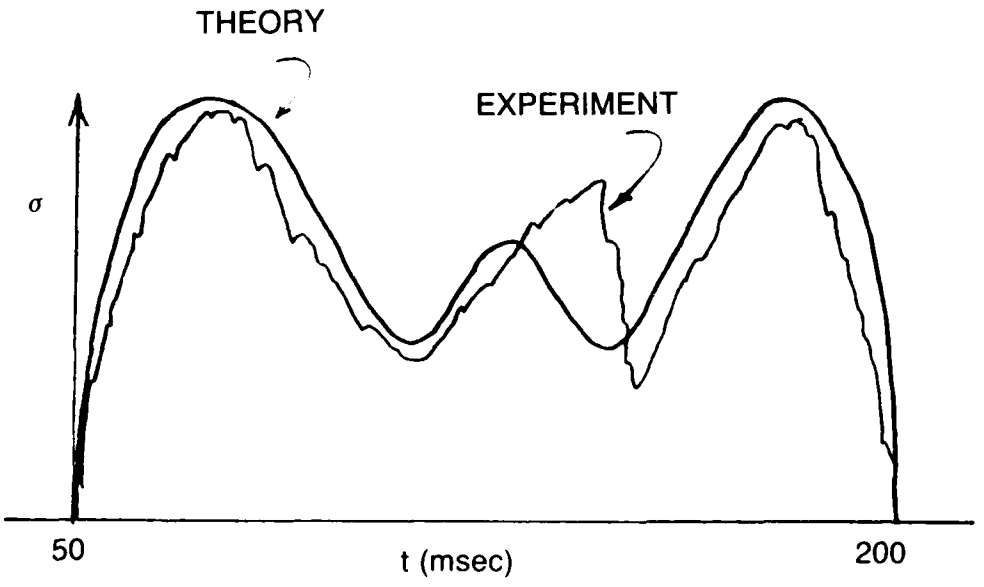

(A = .15MM, F = 10 GHZ, H_{MAX} = 25MM)

b. Comparison of Theory with Experiment

Fig. 14 — Cross Section Variation with Stalk Height for Dielectric Rod Model

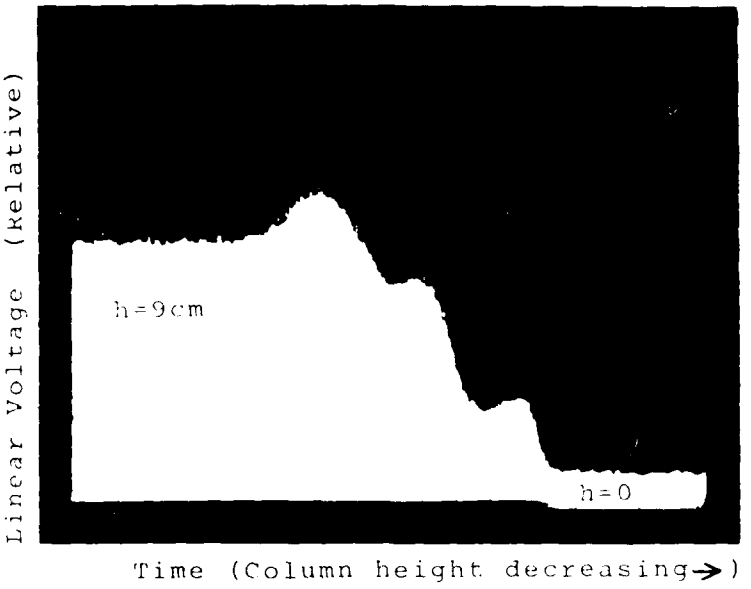

a.) Experimental backscatter from falling water column (grazing angle=27°, diameter=6mm, freq.=10GHz.)

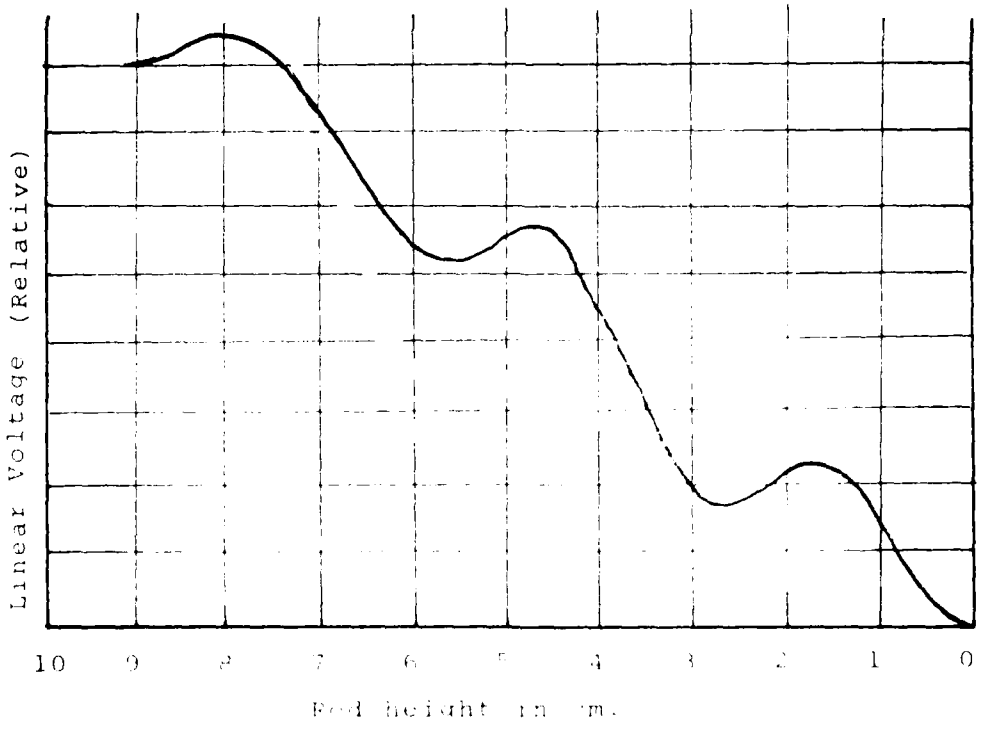

b.) Theoretical backscatter vs. dielectric rod height. (Grazing angle 27°, wavelength free space, f=10GHz.)

Fig. 14 Theory and experiment for water column of varying height

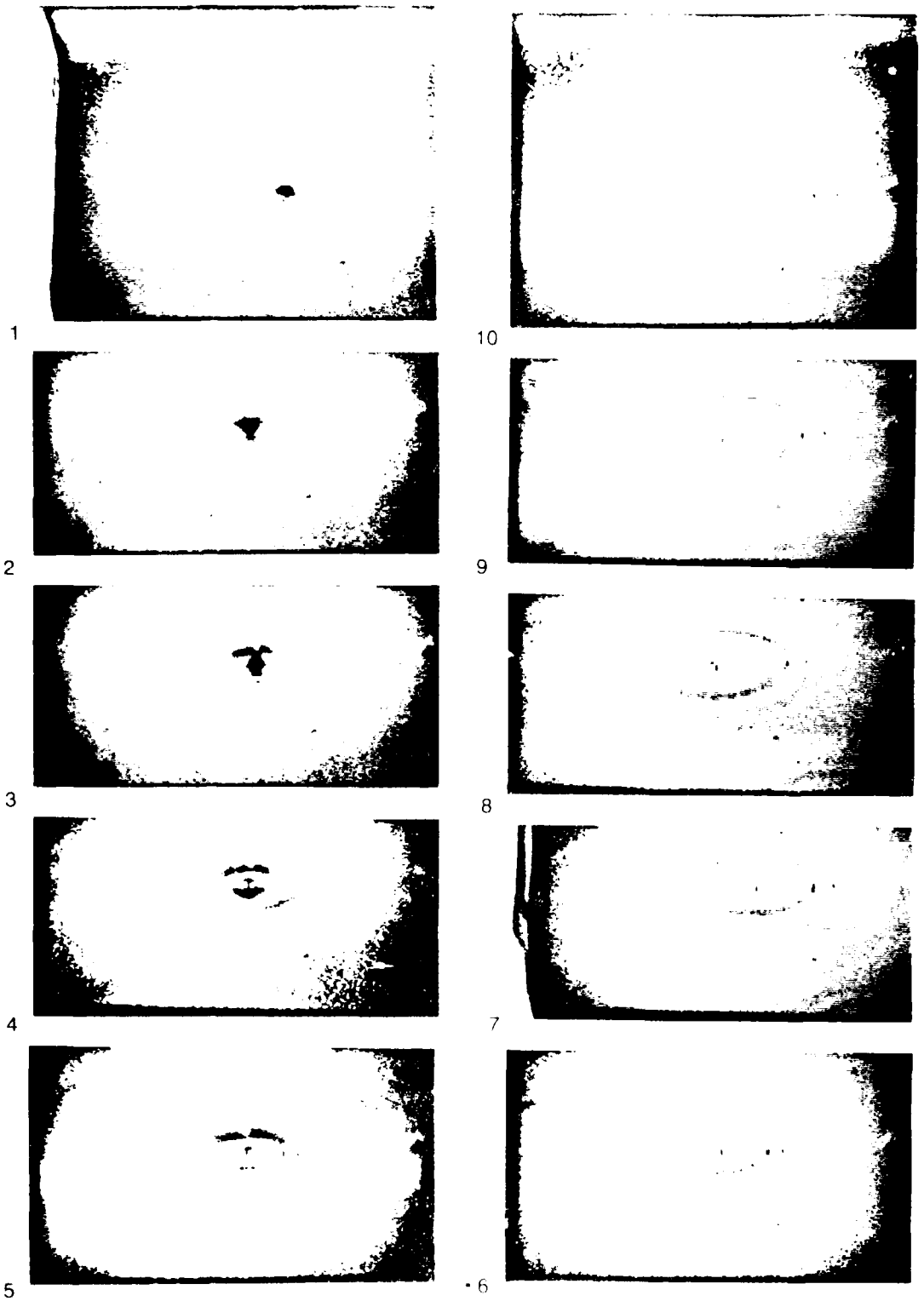

Fig. 15 Video Re[illegible] of the [illegible]on of the Ring Wave

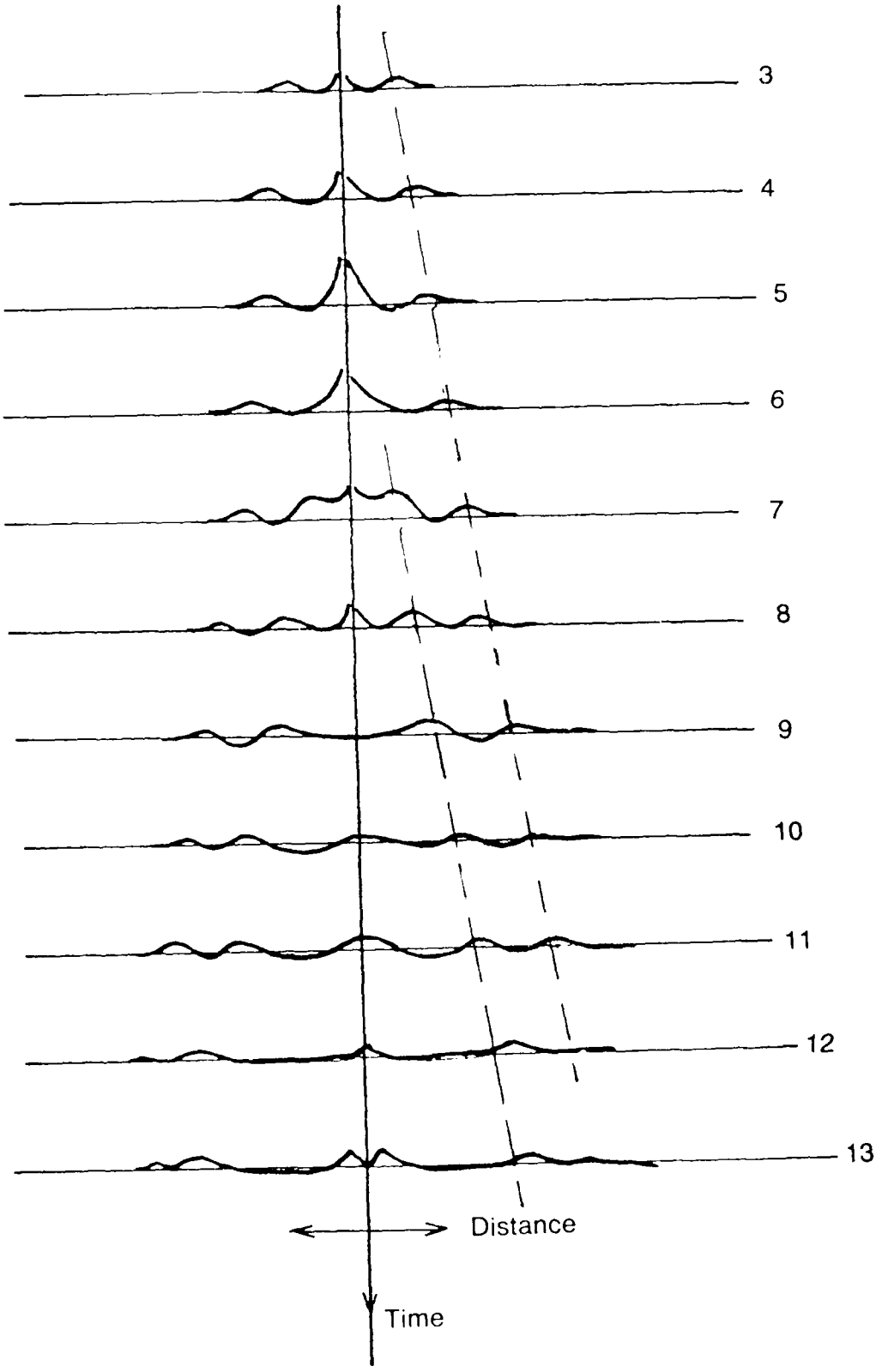

Fig. 16 — Sketch of Sequential Development of the Ring Wave with Time

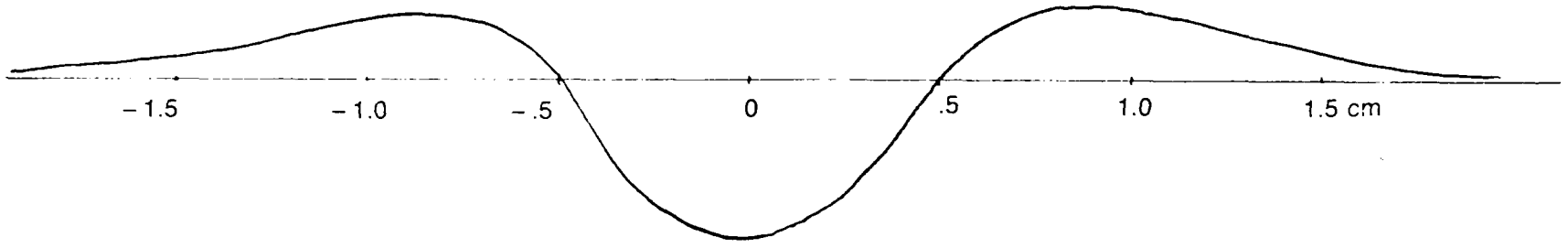

Fig. 17 — Ring Wave Profile based on a Double Gaussian Waveform

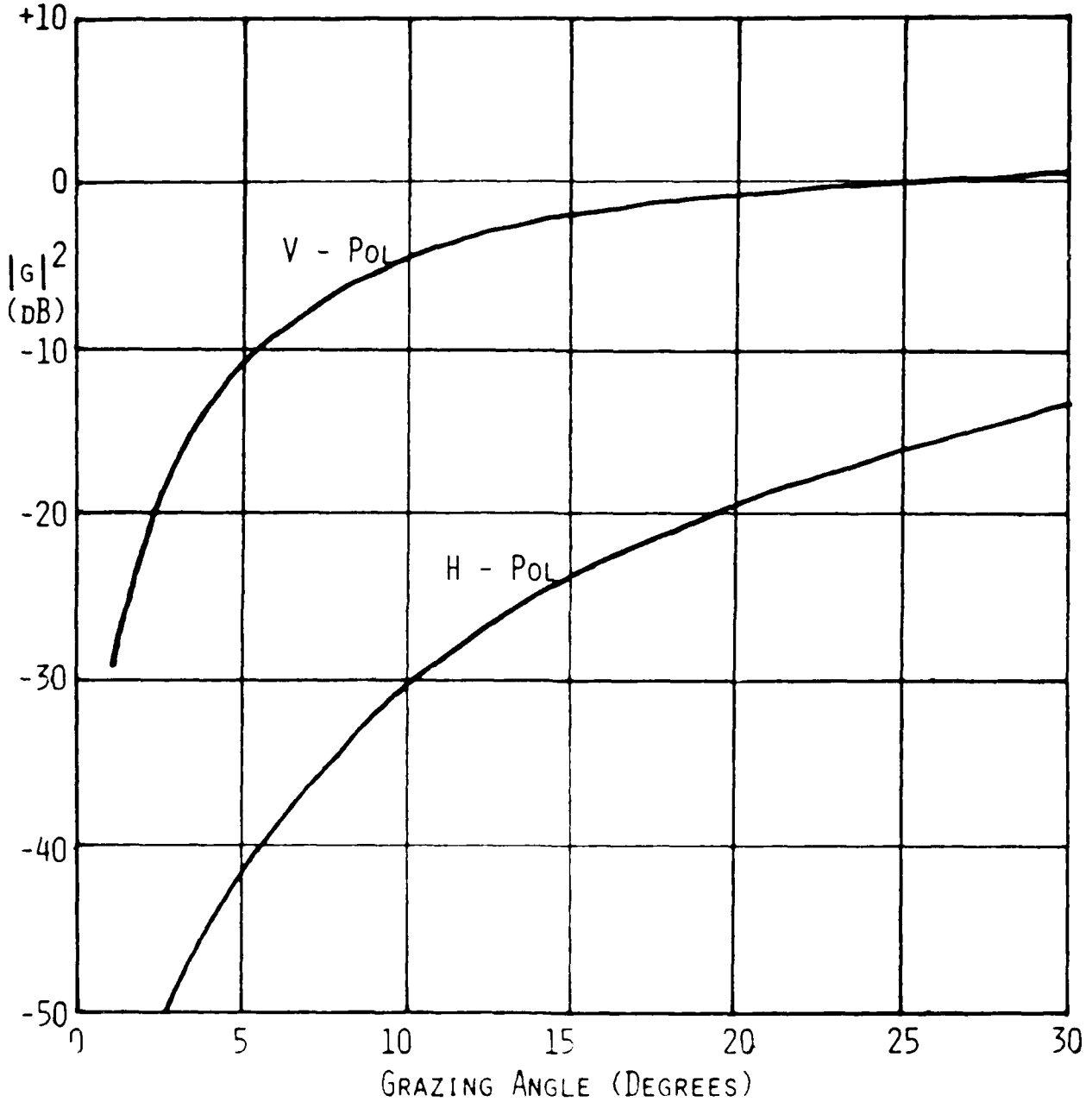

Fig. 18 Angle Factors $|g_{\perp,\parallel}|^2$ in Perturbation Theory

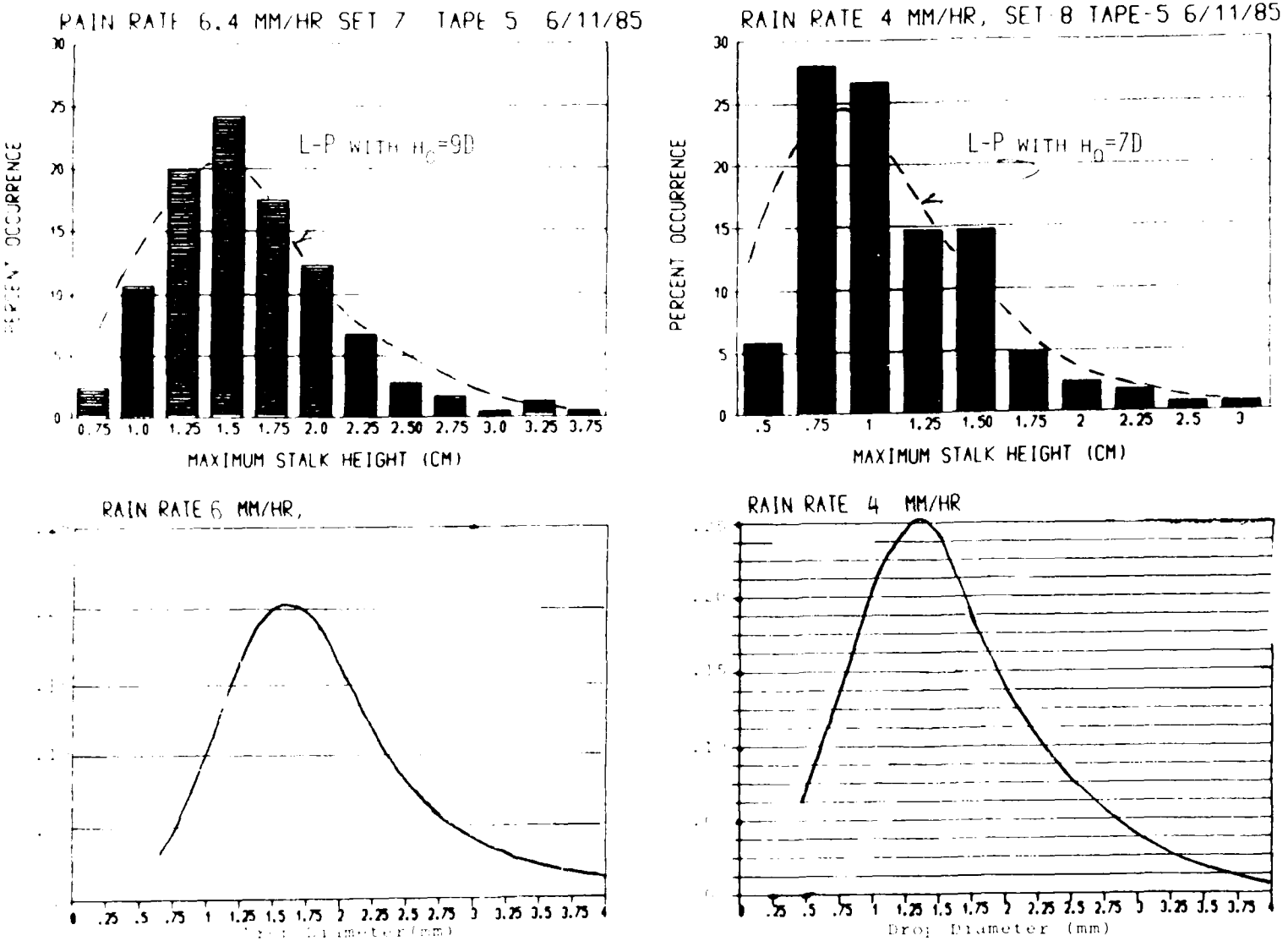

Fig. 19 — Measured Stalk Height Distributions Compared with Laws-Parson Drop Size Distributions

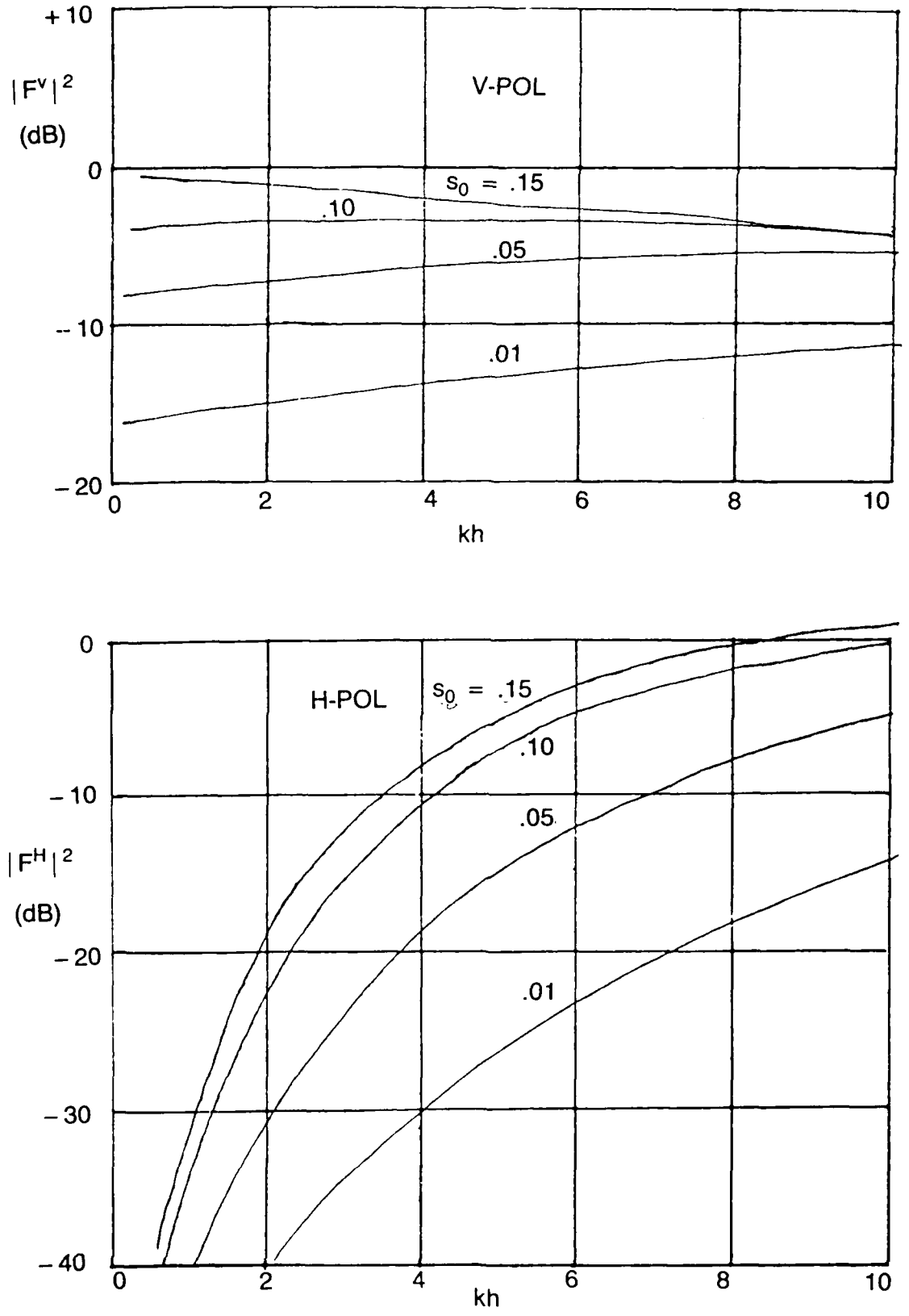

Fig. 20 — Dependence of $|F^{V,H}|^2$ on Surface Slope Distributions ($\psi_0 = 2°$)

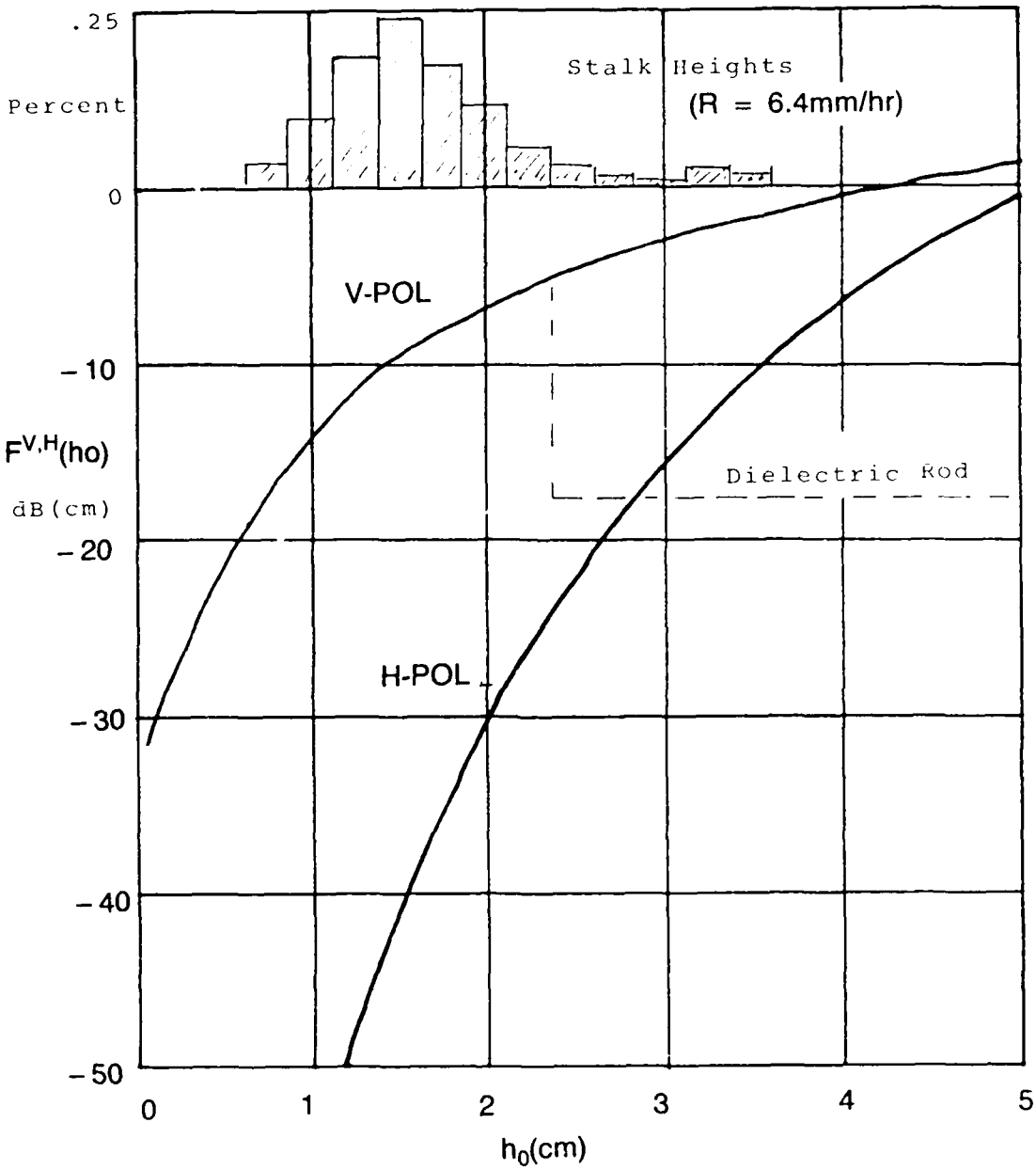

Fig. 21 — Scattering Functions $\mathcal{F}^{V,H}(h_o)$ for $\psi = 2°$, $s_o = 0.1$, $2a = 0.1h_o$, compared with Stalk Height Distribution $p(h_o)$

END

FILMED

MARCH, 1988

DTIC